Decentralized Coordinated Attitude Control of a Formation of Spacecraft

by
Matthew C. VanDyke

Thesis submitted to the Faculty of the
Virginia Polytechnic Institute and State University
in partial fulfillment of the requirements for the degree of

Master of Science
in
Aerospace Engineering

Dr. Christopher D. Hall, Committee Chair
Dr. Hanspeter Schaub, Committee Member
Dr. Naira Hovakimyan, Committee Member

May 21, 2004
Blacksburg, Virginia

Keywords: spacecraft, dynamics, control, decentralized, coordinated, Liaponuv, nonlinear, formation, attitude, behavior-based

Abstract

Decentralized Coordinated Attitude Control of a Formation of Spacecraft

Matthew Clark VanDyke

Spacecraft formations offer more powerful and robust space system architectures than single spacecraft systems. Investigations into the dynamics and control of spacecraft formations are vital for the development and design of future successful space missions. The problem of controlling the attitude of a formation of spacecraft is investigated. The spacecraft formation is modelled as a distributed system, where the individual spacecraft's attitude control systems are the local control agents. A decentralized attitude controller utilizing behavior-based control is developed. The global stability of the controller is proven using Lyaponuv stability theory. Convergence of the attitude controller is proven through the use of an invariance argument. The attitude controller's stability and convergence characteristics are investigated further through numeric simulation of the attitude dynamics of the spacecraft formation.

Dedication & Acknowledgements

I dedicate this work to my beautiful fianceé Melissa, who had to withstand two years of separation from me because of it. How she was ever able to summon the courage and fortitude necessary to withstand such a tremendous sacrifice, I may never know. I also dedicate some small portion of this work (perhaps just the references) to the past and present inhabitants* of the Space Systems Simulation Laboratory, whose ability to divert my attention from my work (with such wonderfully silly things as lunch and demerits) was invaluable in the delay to get it done. I would like to thank my advisor, Dr. Hall, for his guidance in this research and without whom this manuscript would not be the sparkling example of perfection that you see before you. And finally, I would like to thank the Virginia Space Grant Consortium who generously partially funded this research.

*In loose chronological order: Jana Schwartz, Matt Berry, Scott Lennox, Marcus Pressl, Andrew Turner, Eugene Skelton, Mike Shoemaker, Brett Streetman, Sam Wright, Justin McFarland

Contents

List of Figures

List of Tables

Nomenclature

$\vec{\mathbf{v}}$	Vector
$\mathcal{F}$	Reference Frame
$\mathcal{F}_k$	k Reference Frame
$\mathcal{F}_b$	Body-Fixed Reference Frame
$\mathcal{F}_i$	Inertial Reference Frame
$\mathbf{v}_k$	$\vec{\mathbf{v}}$ Expressed in $\mathcal{F}_k$
v_k	kth Component of $\vec{\mathbf{v}}$
$\mathbf{R}$	Rotation matrix
$\mathbf{R}^{jk}$	Rotation matrix representing the rotation from $\mathcal{F}_k$ to $\mathcal{F}_j$
$\angle_{\vec{\mathbf{a}},\vec{\mathbf{b}}}$	Angle Between $\vec{\mathbf{a}}$ and $\vec{\mathbf{b}}$
$\mathbf{1}$	Identity Matrix
$\boldsymbol{\omega}_{jk}$	Angular Velocity of $\mathcal{F}_j$ with respect to $\mathcal{F}_k$ expressed in $\mathcal{F}_j$
$\bar{\mathbf{q}}$	Quaternion
$\mathbf{q}$	Vector Part of the Quaternion
q_4	Scalar Part of the Quaternion
$\mathbf{e}$	Euler Axis
Φ	Euler Angle
$\bar{\mathbf{q}}^{-1}$	Inverse Quaternion
$\vec{\mathbf{h}}$	Angular Momentum Vector
$\mathbf{I}$	Moment of Inertia Matrix
$\hat{\bar{\mathbf{q}}}$	Absolute Desired Attitude Quaternion
$\delta\bar{\mathbf{q}}$	Station-Keeping Attitude Error Quaternion
$\hat{\boldsymbol{\omega}}$	Absolute Desired Angular Velocity Vector
$\delta\boldsymbol{\omega}$	Station-Keeping Angular Velocity Error Vector

$\bar{\mathbf{q}}_{jk}$	Attitude Error Between the jth and kth Spacecraft
$\boldsymbol{\omega}_{jk}$	Angular Velocity Error Between the jth and kth Spacecraft
$\mathbf{g}$	External Control Torque
k_p	Proportional Control Gain
k_d	Derivative Control Gain
$\delta\bar{\mathbf{q}}_j$	Station-Keeping Attitude Error Quaternion for the jth Spacecraft
$\delta\boldsymbol{\omega}_j$	Station-Keeping Angular Velocity Error for the jth Spacecraft
ρ^p_{jk}	Proportional Behavior Weighting Between the jth and kth Spacecraft
ρ^d_{jk}	Derivative Behavior Weighting Between the jth and kth Spacecraft
$\mathbf{g}^s_j$	Station-Keeping Control Action for the jth Spacecraft
$\mathbf{g}^f_j$	Formation-Keeping Control Action for the jth Spacecraft
c	Number of Connections Per Spacecraft in the Formation
$\bar{\mathbf{q}}_k$	Attitude Quaternion of the kth Spacecraft with respect to $\mathcal{F}_i$
$\boldsymbol{\omega}_k$	Angular Velocity of the kth Spacecraft with respect to $\mathcal{F}_i$
$\mathbf{g}_{d_k}$	Disturbance Torque Acting on the kth Spacecraft

Chapter 1

Introduction

The topic of spacecraft formation flying has pervaded much of the recent work in the spacecraft dynamics and control field. The reason for the recent focus is the power and flexibility available to space system architectures that use spacecraft formations. Much of the work has concentrated on translational control of the spacecraft in the formation. However, some work has explored the problem of controlling the attitude of a spacecraft formation. Both centralized and decentralized coordination approaches to the problem have been analyzed. The centralized coordination approaches have been examined in detail;[1–9] however there are still gaps in the decentralized coordination approach literature.[10–14] The most notable gap is the lack of a decentralized coordinated attitude controller that guarantees global convergence of the spacecraft formation. The research presented here extends the previous work in decentralized coordinated attitude control. A class of decentralized coordinated attitude control laws that guarantees global converge of the spacecraft formation is developed and analyzed.

Three basic concepts important in the study of spacecraft formation attitude control are spacecraft formation flying, coordinated control, and behavior-based control. These concepts are briefly introduced and their relevance discussed.

1.1 Spacecraft Formation Flying

A spacecraft formation consists of two or more spacecraft in specific relative positions and orientations. Dispersing the functions of a single spacecraft over a formation of spacecraft produces a robust, fault-tolerant system architecture. The failure of a single spacecraft in a formation does not necessarily lead to system failures as it would in a single, larger spacecraft. Upgrades or repairs could be performed by simply replacing any obsolete or disabled spacecraft.[15] The cost of repair and upgrades of the system is reduced because of the natural modularity of a spacecraft formation.

Spacecraft formations allow for higher performing and more efficient system architectures. A formation facilitates greater resolution through the use of spatially distributed simultaneous measurements.[16] Long-baseline optical interferometry is an example of a high performance system that requires distributed measurements.[17] Another benefit of spacecraft formations is their ability to change the relative spacecraft positions and attitudes to achieve optimal configurations for different missions throughout the lifetime of the system. The result is a system with greater functionality than a system consisting of a single spacecraft.[15]

1.2 Coordinated Control

A spacecraft formation is a distributed system. A distributed system is a large system consisting of multiple smaller subsystems. The attitude control systems of the individual spacecraft act as the local control agents. The control decisions of the local control agents must be coordinated to ensure the stability and convergence of the global system.

Coordinated controllers are generally categorized into centralized and decentralized types. The distinction is based on where the control decisions are made. Centralized control is a type of coordinated control where a single control agent, called the global control agent, determines the control actions for the distributed system. Diagram A of Figure 1.1 shows a block diagram of a distributed system using centralized control. The global control agent commands are represented by the uni-directional arrows directed toward the local control agents.

In decentralized control, control decisions are relegated to the local control agents. The

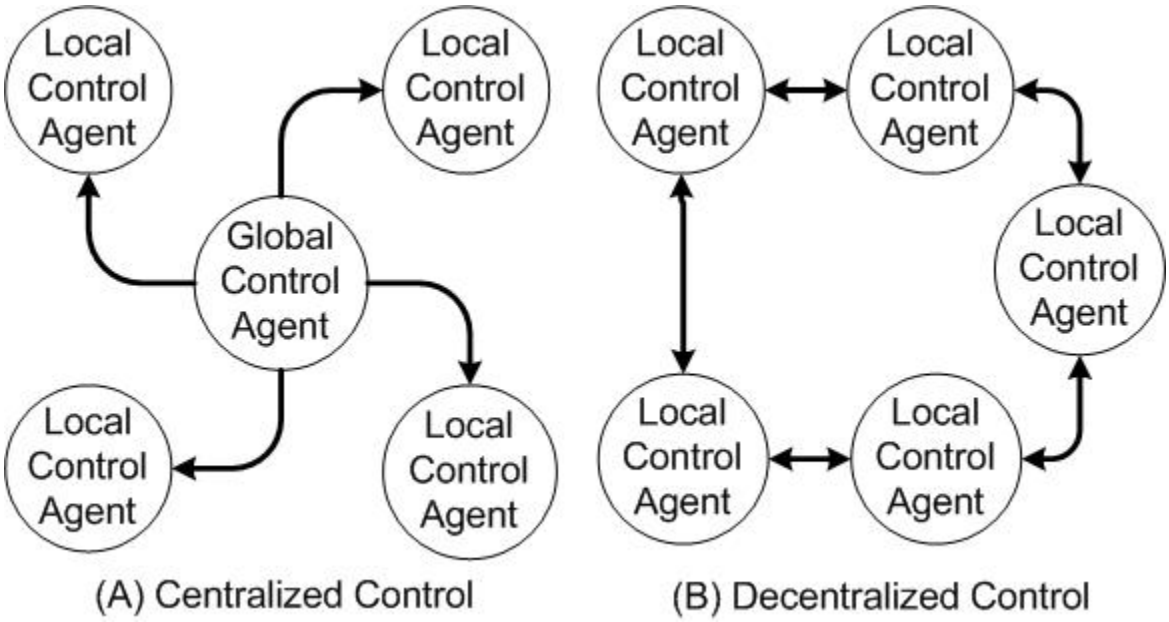

Figure 1.1: A general depiction of the (A) centralized and (B) decentralized coordinated control types.

local control agents use local observations and any information communicated by the other control agents to determine control actions. A block diagram of a distributed system using decentralized control is presented in Part B of Figure 1.1. The bi-directional arrows represent the two-way communication of information between the local control agents.

The two primary benefits of decentralized control over centralized control are fault-tolerance and simpler control laws. Failure of a single local control agent in a decentralized controlled system does not lead to the destabilization of the entire system.[18] The failure is confined to the region of the failed local control agent resulting in a graceful degradation of system performance. Decentralized control results in relatively simple control laws, because the design of the global controller can be decomposed into smaller control agents. The local control agents are designed so that they perform their local control tasks, and coordinate with one another to control the global system.[18] The coordination is implemented by means of communication between the local control agents. Centralized controllers require greater information and information processing than what is required by the local control agents of the equivalent decentralized controller.[19] The primary drawback of decentralized controllers is that they are difficult to analyze analytically.

1.3 Behavior-Based Control

A useful tool for the spacecraft formation attitude control problem is behavior-based control. Behavior-based control is implemented when a control system has multiple, and sometimes competing, objectives or behaviors. The behaviors could include goal-attainment, collision-avoidance, obstacle-avoidance, and formation-keeping. The overall control action is determined by a weighted sum of the control actions for each of the behaviors.[20]

Figure 1.2 shows a situation where the control system of an autonomous vehicle must reconcile conflicting behaviors. The autonomous vehicle is represented by the blue triangle. The red circle is the goal that the vehicle is endeavoring to reach. The gray rectangle is an obstacle that is blocking the most direct path of the vehicle to the goal. The vehicle control system is tasked with simultaneously avoiding obstacles and reaching the goal. The black line is a safe path from the current position to the goal. The path is a compromise between the two conflicting behaviors.

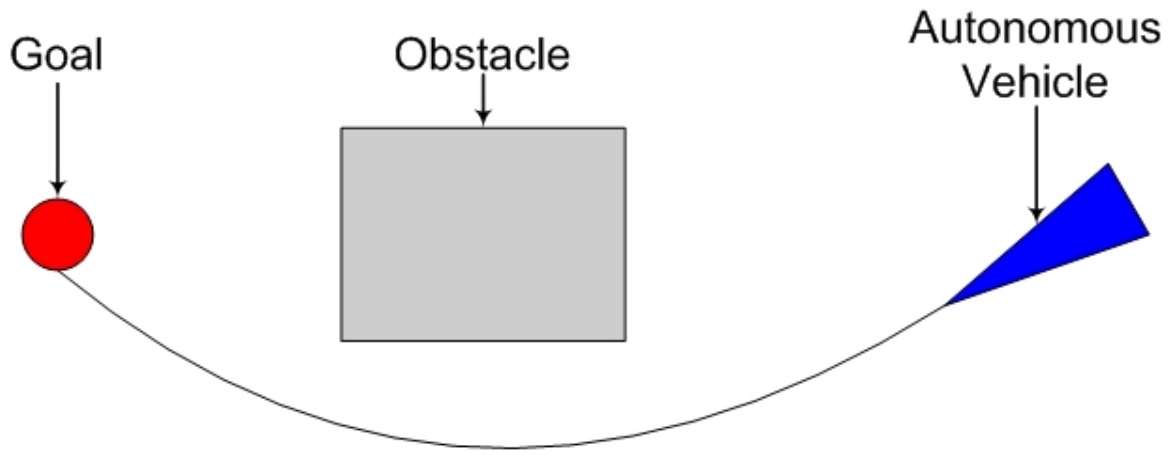

Figure 1.2: An example where a goal attainment behavior and an obstacle avoidance behavior conflict.

For the coordinated attitude control problem, behavior-based control is used to arrive at a compromise between the control actions required for the formation-keeping and station-keeping behaviors.[13] Station-keeping is the behavior that tries to drive the spacecraft to its absolute desired attitude. Formation-keeping is the behavior that tries to align the spacecraft with the other spacecraft in the formation.

1.4 Applications

Research into coordinated attitude control algorithms is applicable to any spacecraft formation flying mission. Improvements in attitude control generally lead to heightened overall system performance. Two interesting applications of this research are long baseline interferometry and spacecraft positional formation-keeping.

1.4.1 Interferometry

Interferometry is being considered as a method to detect extra-solar planets for the Terrestrial Planet Finder (TPF). Interferometry would allow the cancellation of exo-zodiacal light from the planet's signal, thereby providing a better signal from which scientific data can be extracted. One of the concepts being considered for the TPF uses a formation of free-flying spacecraft, separated by hundreds of meters, equipped with optical sensors acting as an interferometer.[21]

Interferometry using a spacecraft formation would require two or more spacecraft to move within an observation plane to reflect light sampled from a celestial body to another spacecraft. Scientific data can then be extracted from the interference pattern of the sampled light.[10] A free-flying spacecraft interferometer provides better performance than a structurally connected interferometer by allowing greater baselines, leading to greater resolutions, and more complex nulling patterns to better cancel unwanted light.[21]

1.4.2 Spacecraft Orbital Formation-Keeping

Coordinated attitude control allows spacecraft in Low Earth Orbit (LEO) to maintain tighter formations. Spacecraft formations in LEO are subject to an atmospheric drag force. The drag force has a disturbing influence on spacecraft formations. Even if the spacecraft are identical, the drag force experienced by each is slightly different. The difference is caused by the relative attitude tracking errors of the spacecraft. The relative attitude error causes the spacecraft to have different attitudes with respect to their velocity vectors, and therefore with respect to the free-stream. The differences in the attitudes of the spacecraft with respect to the free-stream results in differing drag forces. Therefore, a spacecraft formation

with smaller relative attitude error is less affected by the drag force disturbance, thereby lessening the propulsive force required to maintain the formation.[22]

1.5 Outline of Thesis

A review of the literature specifically related to the topic of coordinated attitude control is presented in Chapter 2. The literature is grouped into three categories based on the approach used by the authors. Deficiencies in the literature are noted for later resolution.

A review of spacecraft dynamics is given in Chapter 3. Absolute and relative attitude kinematic error variables for the spacecraft are formulated. Chapter 4 discusses nonlinear attitude control of a spacecraft modelled as a rigid body. Stability definitions and theorems are introduced and used to develop two quaternion-based attitude controllers. The primary contribution of this work is the development and analysis of a class of decentralized attitude controllers that globally asymptotically stabilizes the spacecraft formation, and it is presented in Chapter 5.

Numeric simulations are used in Chapter 6 to validate the analytic results and examine the effects of varying several vital parameters. Finally, conclusions are drawn in Chapter 7 based on the analytic and numeric results presented in Chapters 5 and 6. Areas requiring further investigation are also noted.

Chapter 2

Literature Review

Spacecraft formation flying has been prominent in recent spacecraft dynamics and control literature. The majority of the papers on the subject focus on the problem of controlling and maintaining the relative positions of the spacecraft in the formations. However, several papers have investigated the problem of controlling and maintaining the relative attitudes of the spacecraft in the formation. Work in the coordinated attitude control area has been produced primarily by three schools. The first school investigates leader-follower type coordination strategies. The papers of the second school concentrate on behavior-based and virtual structure coordination strategies. The third school uses a fundamentally different approach than the first two schools, where the control law and the coordination layer are decoupled.

2.1 Wang, Hadaegh, Yee, and Lau - The First School

One of the first school's earlier coordinated attitude control papers is by Wang and Hadaegh.[1] Their paper investigates the use of one-leader, multiple-leader, and barycenter coordination strategies. The one-leader coordination strategy requires that one spacecraft serves as the reference spacecraft, the leader, for the rest of the spacecraft, the followers, in the formation. The followers then track the leader, possibly with a constant offset. The multiple-leader approach involves splitting the formation into two or more groups and assigning one or more fleet leaders. The fleet leaders act as the reference spacecraft for the group leaders, which

in turn, act as the reference spacecraft for the group followers. This approach results in a hierarchical communication topology. The most interesting coordination strategy discussed is the barycenter strategy. In this strategy, the ith spacecraft uses the position information of the neighboring spacecraft to determine the barycenter of their locations. The barycenter is then used as the desired location of the ith spacecraft.

The authors develop control laws for position control for each of these coordination strategies, and prove globally asymptotically stability of the closed-loop system. Disappointingly, only one type of coordination strategy is investigated for attitude control of the formation. A nearest-neighbor attitude controller is developed and proven to globally asymptotically stabilize the attitude of the spacecraft formation. The nearest-neighbor controller uses a leader-follower coordination architecture with multiple leaders. The nearest-neighbor attitude controller uses a "chain" coordination architecture, where each spacecraft follows one other spacecraft in the formation, except the leader who tracks the absolute desired attitude trajectory of the formation.

In a subsequent paper, Wang, Hadaegh, and Lau[2] use the same type of formulation to develop one-leader based coordinated control laws for position and attitude control of a spacecraft formation. The interesting addition of this paper is the application of the one-leader coordinated control strategy to the problem of Michelson stellar interferometry. A more recent paper by Wang, Lee and Hadaegh[3] implements the one-leader coordination strategy for attitude control on an experimental spacecraft attitude dynamics simulator system.

2.2 Lawton, Beard, Hadaegh, and Ren - The Second School

The second school of researchers uses an approach that is similar to the first school; however they investigate more exotic methods for coordinated control. However, Lawton, Beard, and Hadaegh[10] develop a relatively simple leader-follower coordinated controller to be used primarily as a baseline for which to compare the performance of their behavior-based and virtual structure coordinated controllers.

Lawton, Beard, and Hadaegh[10] develop a decentralized controller for the spacecraft formation

attitude control problem that they term the coupled dynamics controller. The coupled dynamics controller uses a ring communication topology, where each spacecraft knows the state of two other spacecraft in the formation. The desired state and the state of the two other spacecraft are used to determine the appropriate control torque. A convergence proof is provided; however the proof does not ensure global convergence of the formation attitude. It requires that the spacecraft begin with no angular rate and that the initial formation error is below a certain limit. Appendix B of the paper gives an interesting proof demonstrating that the geodesic metric between two unit quaternions can be approximated by the Euclidean distance between them, which is a useful result for developing formation attitude error measures.

In another paper, Lawton and Beard[14] develop a passivity-based controller for the spacecraft formation attitude control problem. The passivity-based controller uses only attitude information to determine control actions, thus alleviating the need for angular rate measurements. The authors also analytically determine the domain of attraction for the passivity-based controller and the coupled dynamics controller.

The coupled dynamics and passivity-based controllers use behavior-based control. Behavior-based control is used in the literature because it is a method of reconciling sometimes conflicting control aims or behaviors. The control aim conflict of the attitude control system of a spacecraft in a formation is that it must simultaneously try to align the spacecraft with its absolute desired attitude and with the other spacecraft in the formation.

A more general architecture for spacecraft formation attitude control is introduced by the same authors in a later paper.[13] The architecture is designed to subsume the leader-follower, behavior-based, and virtual-structure coordination strategies. The authors claim that the architecture is "amenable to analysis via control theoretic methods." A brief descriptive list of some formation control problems that can be analyzed using the architecture is given. The authors demonstrate the usefulness of the architecture by applying it to the practical problem of Michelson stellar interferometry. The problem is solved by defining the different modes that are required by the interferometry system, and using the general architecture to develop an appropriate controller for each mode.

Ren and Beard[9] investigate a centralized implementation of virtual structure coordination strategy using the general architecture. The primary contribution of the paper is the addition of formation feedback to the spacecraft formation. The authors prove the virtual structure

control law guarantees the stability and convergence of the system.

2.3 Kang, Yeh, and Sparks - The Third School

The approach to the design of coordinated controllers by the third school is far different from the approaches used by the first two schools. The third school completely decouples the individual attitude controllers from the coordinated controller. The goal of the third school is also slightly different. The first two schools strive to guarantee convergence of the formation, whereas the third school looks to only stabilize the formation to a final state that minimizes the relative and absolute errors of the spacecraft in the presence of tracking errors.

A coordinated controller based on decentralized feedback is introduced by Kang, Yeh, and Sparks.[7] A reference projection is used to determine the appropriate control action for the spacecraft. Each spacecraft in the formation uses its current desired state and state information communicated by the other spacecraft to determine a quasi-desired state using the reference projection. The quasi-desired state is then used by the spacecraft's attitude controller to determine the appropriate control action.

Different types of coordination are possible using the appropriate reference projection. In the paper, a reference projection is developed for the leader-follower, generalized leader-follower, and the virtual desired attitude coordination strategies. The leader-follower reference projection for the leader is the desired state of the formation, and the current state of the leader is the reference projection for the follower spacecraft. The generalized leader-follower strategy differs in that the reference projection for the followers is a compromise between the desired state and the current state of the leader. The only truly decentralized coordination strategy is the virtual desired attitude strategy, where the reference projection for each spacecraft is a compromise between the desired state and the average state of the spacecraft in the formation.

In a later paper, Kang and Yeh[5] first discuss applying the idea of reference projections to tracking control. Kang and Sparks[8] investigate the idea further and present simulation results.

2.4 Deficiencies in the Literature

Coordinated attitude control is a relatively new topic in the spacecraft dynamics and control field. The literature on the topic uses some interesting and novel methods to attack the coordinated control problem, such as behavior-based control and reference projections. However, the literature suffers from two glaring deficiencies. The first is the poor definition of kinematic error variables used in the development of the coordinated controllers, and the second is the lack of global stability and convergence proofs for the decentralized coordinated controllers.

The kinematic attitude error quantities used by the authors of the first and third school are simply differences between quaternions or angular velocity vectors, in different reference frames. The second school defines a proper relative attitude quaternion, but does not define a proper relative angular velocity vector. The fundamentally nonlinear nature of rotational kinematics is ignored. The difference of two quaternions or two angular velocity vectors, that are not in the same reference frame, is not a physically significant quantity.

Despite the use of poorly defined, valid analytic proofs are provided by all three schools. Authors from the first and seconds schools offer global stability and convergence proofs for centralized leader-follower type coordinated controllers. Local analytic stability and convergence proofs are offered by authors from the second school for their decentralized coupled dynamics controller. The third school also offers a local stability proof for its reference projection based coordinated attitude controllers. However, analytic proofs of global stability and convergence for decentralized coordinated controllers do not appear in the literature.

2.5 Summary and Conclusions

The deficiencies of the literature noted here are addressed and resolved by this work. Proper kinematic error variables that recognize the nonlinearity of rotational kinematics are defined and used in the development of decentralized attitude controllers. The stability and convergence characteristics of decentralized controllers are investigated in greater depth.

Chapter 3

Spacecraft Attitude Dynamics

The topic of spacecraft attitude dynamics is briefly reviewed in this chapter. The basic concepts of vectors, reference frames, and attitude are introduced and defined. Two attitude representations used in this work, rotation matrices and quaternions, are introduced and defined. The attitude dynamics equations of motion are briefly derived under the assumption that the spacecraft is a rigid body. Absolute and relative attitude kinematic variables for the spacecraft formation attitude control problem are developed. The concepts and equations developed in this chapter are used extensively in the analysis and simulation of the attitude controllers in later chapters.

3.1 Vectors and Reference Frames

A vector is a mathematic quantity in three-dimensional space possessing both magnitude and direction.[23] A bold lowercase letter with an arrow above it denotes a vector, $\vec{\mathbf{v}}$. A reference frame, $\mathcal{F}$, is defined as a dextral, orthonormal triad.[23–25] A triad is a set of three unit vectors. The orthonormal and dextral adjectives restrict the vectors in the triad to be mutually perpendicular and right-handed. Figure 3.1 is a diagram of the k reference frame, $\mathcal{F}_k$.

Two reference frames that are important in attitude dynamics are the inertial reference frame, $\mathcal{F}_i$, and the body-fixed reference frame, $\mathcal{F}_b$. The inertial reference frame is a non-rotating and non-accelerating reference frame. The inertial reference frame is useful because some

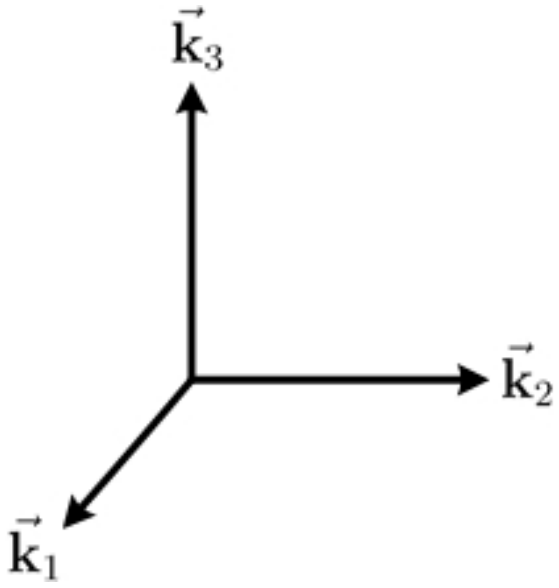

Figure 3.1: The kth reference frame, $\mathcal{F}_k$, consisting of the triad of $\vec{\mathbf{k}}_1$, $\vec{\mathbf{k}}_2$, and $\vec{\mathbf{k}}_3$

quantities with respect to this reference frame are constant or conservative. The body-fixed reference frame is useful in developing the attitude dynamics equations of motion because the moments of inertia of a rigid body expressed in $\mathcal{F}_b$ are constant.[23–25]

A vector can be defined as the sum of its projections on the three reference unit vectors of a reference frame,

$$\vec{\mathbf{v}} = v_1\vec{\mathbf{k}}_1 + v_2\vec{\mathbf{k}}_2 + v_3\vec{\mathbf{k}}_3 \tag{3.1}$$

where v_1, v_2, and v_3 are the projections of $\vec{\mathbf{v}}$ onto the reference vectors of $\mathcal{F}_k$, $\vec{\mathbf{k}}_1$, $\vec{\mathbf{k}}_2$, and $\vec{\mathbf{k}}_3$.[23–25] A vector can be represented in a given reference frame using a three element column matrix,

$$\mathbf{v}_k = \begin{bmatrix} v_1 & v_2 & v_3 \end{bmatrix}^{\mathsf{T}} \tag{3.2}$$

where $\mathbf{v}_k$ is a column matrix representation of $\vec{\mathbf{v}}$. The subscript k denotes that the representation is expressed in $\mathcal{F}_k$. Figure 3.2 depicts a vector, $\vec{\mathbf{v}}$, in $\mathcal{F}_k$. The omission of a subscript for the column matrix representation of a vector denotes that the vector is expressed in $\mathcal{F}_b$.

A vector can be represented in an infinite number of reference frames. The reference frames differ in their orientation or attitude with respect to one another. It is therefore important to be able to rotate a vector from its representation in one reference frame to its representation

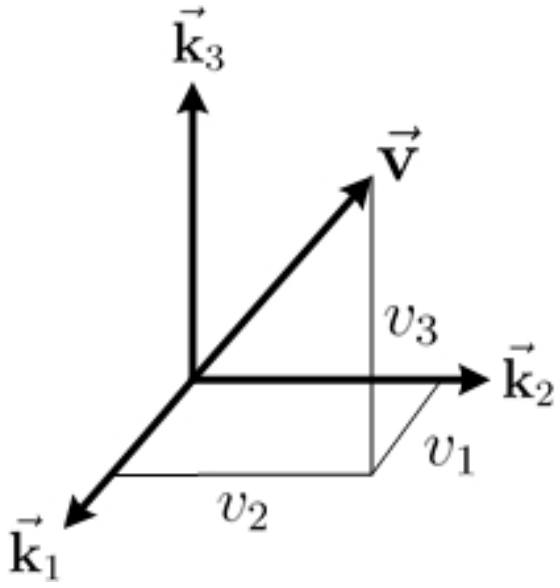

Figure 3.2: The vector $\vec{\mathbf{v}}$ shown in the kth reference frame, $\mathcal{F}_k$

in another. In the next section, mathematical constructs for defining orientations of reference frames are introduced.

3.2 Attitude Representations

Attitude representations are used to define the orientation of one reference frame with respect to another reference frame. The two attitude representations used in this work are rotation matrices and quaternions. Rotation matrices are used to rotate vectors expressed in one reference frame to be expressed in another reference frame. Quaternions are used to represent the absolute attitude of the spacecraft for the development of the attitude controllers in the next chapter.

3.2.1 Rotation Matrices

A rotation matrix, $\mathbf{R}$, is a 3×3 matrix that represents the attitude of one reference frame with respect to another.[23–25] For clarity, superscripts are used to denote the two reference frames. $\mathbf{R}^{jk}$ is the rotation matrix that represents the rotation from $\mathcal{F}_k$ to $\mathcal{F}_j$. Figure 3.3

depicts the relative orientations or attitude of the two reference frames.

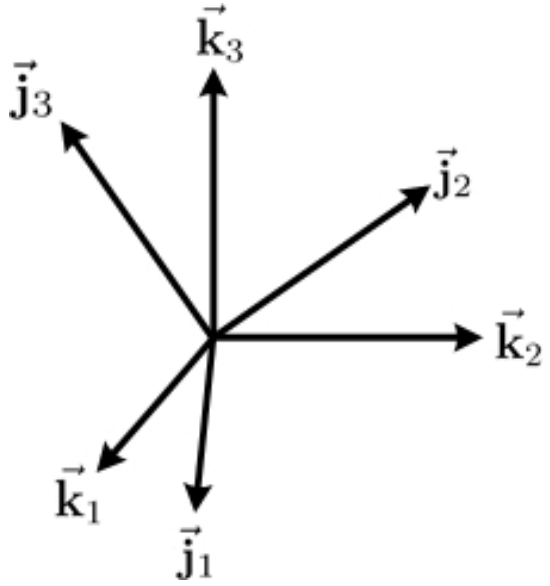

Figure 3.3: The unit reference vectors of $\mathcal{F}_j$ and $\mathcal{F}_k$

A rotation matrix can be defined in terms of the reference vectors of the two reference frames using

$$\mathbf{R}^{jk} = \begin{bmatrix} \mathbf{j}_{k,1} & \mathbf{j}_{k,2} & \mathbf{j}_{k,3} \end{bmatrix} = \begin{bmatrix} \mathbf{k}_{j,1} \\ \mathbf{k}_{j,2} \\ \mathbf{k}_{j,3} \end{bmatrix} \tag{3.3}$$

where $\mathbf{j}_{k,l}$ is $\vec{\mathbf{j}}_l$ expressed in $\mathcal{F}_k$. From this formulation it is easy to determine that the rotation matrix that represents the inverse rotation of $\mathbf{R}^{jk}$ is

$$\mathbf{R}^{kj} = \left(\mathbf{R}^{jk}\right)^{\mathsf{T}} \tag{3.4}$$

A rotation matrix can also be defined by the cosines of the angles between the reference unit vectors of the two reference frames using[23–25]

$$\mathbf{R}^{jk} = \begin{bmatrix} \cos\left(\angle_{\vec{\mathbf{j}}_1,\vec{\mathbf{k}}_1}\right) & \cos\left(\angle_{\vec{\mathbf{j}}_1,\vec{\mathbf{k}}_2}\right) & \cos\left(\angle_{\vec{\mathbf{j}}_1,\vec{\mathbf{k}}_3}\right) \\ \cos\left(\angle_{\vec{\mathbf{j}}_2,\vec{\mathbf{k}}_1}\right) & \cos\left(\angle_{\vec{\mathbf{j}}_2,\vec{\mathbf{k}}_2}\right) & \cos\left(\angle_{\vec{\mathbf{j}}_2,\vec{\mathbf{k}}_3}\right) \\ \cos\left(\angle_{\vec{\mathbf{j}}_3,\vec{\mathbf{k}}_1}\right) & \cos\left(\angle_{\vec{\mathbf{j}}_3,\vec{\mathbf{k}}_2}\right) & \cos\left(\angle_{\vec{\mathbf{j}}_3,\vec{\mathbf{k}}_3}\right) \end{bmatrix} \tag{3.5}$$

where $\angle_{\vec{\mathbf{j}}_l,\vec{\mathbf{k}}_m}$ is the angle between the lth reference vector of $\mathcal{F}_j$ and the mth reference vector of $\mathcal{F}_k$. The rotation matrix is also referred to as the direction cosine matrix, because of this formulation, Eq. (3.5).

The rotation matrix attitude representation provides a simple method for adding successive rotations using matrix multiplication. The rotation matrix representing the successive rotations of $\mathbf{R}^{jk}$ and $\mathbf{R}^{lj}$ is found using

$$\mathbf{R}^{lk} = \mathbf{R}^{lj}\mathbf{R}^{jk} \tag{3.6}$$

The interior superscripts of the rotation matrices being multiplied are effectively cancelled. Using Eqs. (3.4) and (3.6), the transpose of a rotation matrix is found to be equal to its inverse,

$$\mathbf{R}^{jk}\left(\mathbf{R}^{jk}\right)^{\mathsf{T}} = \mathbf{R}^{jk}\mathbf{R}^{kj} = \mathbf{R}^{jj} = \mathbf{1} \tag{3.7}$$

where $\mathbf{1}$ is the identity matrix.

Rotation matrices are used to rotate a vector expressed in one reference frame to be expressed in another reference frame. The vector $\vec{\mathbf{v}}$ as expressed in $\mathcal{F}_j$, $\mathbf{v}_j$, can be calculated using

$$\mathbf{v}_j = \mathbf{R}^{jk}\mathbf{v}_k \tag{3.8}$$

where $\mathbf{v}_k$ is $\vec{\mathbf{v}}$ as expressed in $\mathcal{F}_k$.

Equations defining time development of the rotation matrix are required in the development of the attitude tracking control laws. The first time derivative of the rotation matrix is defined

$$\dot{\mathbf{R}}^{jk} = -\boldsymbol{\omega}_{jk}^{\times}\mathbf{R}^{jk} \tag{3.9}$$

where $\boldsymbol{\omega}_{jk}$ is the angular velocity of $\mathcal{F}_j$ with respect to $\mathcal{F}_k$ expressed in $\mathcal{F}_j$. The superscript operator $\times$ denotes the skew-symmetric matrix given by

$$\mathbf{v} = \begin{bmatrix} v_1 \\ v_2 \\ v_3 \end{bmatrix} \Leftrightarrow \mathbf{v}^{\times} = \begin{bmatrix} 0 & -v_3 & v_2 \\ v_3 & 0 & -v_1 \\ -v_2 & v_1 & 0 \end{bmatrix} \tag{3.10}$$

Rotation matrices will be used in the development of the relative angular velocity vector later in this chapter, and throughout the derivations of the attitude control laws presented in the next two chapters.

3.2.2 Quaternions

The attitude of the spacecraft in the formation is represented using the quaternion. The quaternion is a four-element column matrix that is defined in terms of the Euler angle and Euler axis of the rotation it represents. Euler's theorem states that any pure rotational displacement can be generalized into a unit vector, Euler axis, defining the axis of the rotation and an angle, Euler angle, defining the magnitude of the rotation.[23–25] The quaternion, $\bar{\mathbf{q}}$, is defined as

$$\bar{\mathbf{q}} = \begin{bmatrix} \mathbf{e}\sin\left(\frac{\Phi}{2}\right) \\ \cos\left(\frac{\Phi}{2}\right) \end{bmatrix} = \begin{bmatrix} \mathbf{q} \\ q_4 \end{bmatrix} \tag{3.11}$$

where $\mathbf{e}$ is the Euler axis, Φ is the Euler angle, $\mathbf{q}$ is the vector part, and q_4 is the scalar part of the quaternion. The quaternion is related to the rotation matrix that represents the equivalent rotation using

$$q_4 = \pm\frac{1}{2}\sqrt{1+\text{trace}\left(\mathbf{R}\right)} \tag{3.12}$$

$$\mathbf{q} = \frac{1}{4q_4}\begin{bmatrix} R_{23}-R_{32} \\ R_{31}-R_{13} \\ R_{12}-R_{21} \end{bmatrix} \tag{3.13}$$

and,

$$\mathbf{R}\left(\bar{\mathbf{q}}\right) = q_4^2\mathbf{1} + 2\mathbf{q}\mathbf{q}^{\mathsf{T}} - 2q_4\mathbf{q}^{\times} \tag{3.14}$$

Numeric subscripts, such as q_4 represent the corresponding component of the quaternion. Single subscripts, $\bar{\mathbf{q}}_a$, represent the attitude of corresponding reference frame, $\mathcal{F}_a$, with respect to the inertial reference frame, $\mathcal{F}_i$. Similar to the notation for rotation matrices, double subscripts on quaternions are used to clearly denote the rotation represented by the quaternion (e.g. $\mathbf{R}\left(\bar{\mathbf{q}}_{br}\right) = \mathbf{R}^{br}$).

The definition of the quaternion is restricted here so that

$$q_4 \geq 0 \tag{3.15}$$

The restriction is required to account for the ambiguity in the quaternion representation that allows $\bar{\mathbf{q}}$ and $-\bar{\mathbf{q}}$ to represent the same rotation. The restriction leads to the unambiguous definition of the inverse quaternion,

$$\bar{\mathbf{q}}^{-1} = \begin{bmatrix} -q_1 & -q_2 & -q_3 & q_4 \end{bmatrix}^{\mathsf{T}} \tag{3.16}$$

which represents the equal and opposite rotation represented by $\bar{\mathbf{q}}$. The inverse quaternion has the property that

$$\mathbf{R}\left(\bar{\mathbf{q}}\right)\mathbf{R}\left(\bar{\mathbf{q}}^{-1}\right) \;=\; \mathbf{1} \tag{3.17}$$

Like the rotation matrix, the quaternion has a straight-forward method to mathematically "add" successive rotations called quaternion multiplication. The quaternion that represents the successive rotations of $\bar{\mathbf{q}}_b$ and $\bar{\mathbf{q}}_a$ is

$$\bar{\mathbf{q}}_c \;=\; \bar{\mathbf{q}}_a \otimes \bar{\mathbf{q}}_b \tag{3.18}$$

where $\otimes$ is the operator for quaternion multiplication. The $\otimes$ operator is defined as

$$\bar{\mathbf{q}}_c \;=\; \begin{bmatrix} q_{4,a} & q_{3,a} & -q_{2,a} & q_{1,a} \\ -q_{3,a} & q_{4,a} & q_{1,a} & q_{2,a} \\ q_{2,a} & -q_{1,a} & q_{4,a} & q_{3,a} \\ -q_{1,a} & -q_{2,a} & -q_{3,a} & q_{4,a} \end{bmatrix} \begin{bmatrix} q_{1,b} \\ q_{2,b} \\ q_{3,b} \\ q_{4,b} \end{bmatrix} \tag{3.19}$$

Quaternion multiplication is used extensively in the development of attitude error measures later in this chapter.

The first time derivative of the quaternion is defined as

$$\dot{\bar{\mathbf{q}}} \;=\; \frac{1}{2}\,\bar{\boldsymbol{\omega}} \otimes \bar{\mathbf{q}} \tag{3.20}$$

where $\bar{\boldsymbol{\omega}}$ is defined

$$\bar{\boldsymbol{\omega}} \;=\; \begin{bmatrix} \boldsymbol{\omega} & 0 \end{bmatrix}^{\mathsf{T}} \tag{3.21}$$

and $\boldsymbol{\omega}$ is the angular velocity of the spacecraft. The omission of reference frame subscripts denotes that $\boldsymbol{\omega}$ is the angular velocity of $\mathcal{F}_b$ with respect to $\mathcal{F}_i$ expressed in $\mathcal{F}_b$.

3.3 Equations of Motion

The individual spacecraft in the formation are modelled as rigid bodies. The angular momentum, $\mathbf{h}$, of a spacecraft about its mass center with respect to inertial space is[24]

$$\mathbf{h} \;=\; \mathbf{I}\boldsymbol{\omega} \tag{3.22}$$

where $\mathbf{I}$ is the moment of inertia matrix of the spacecraft expressed in $\mathcal{F}_b$. The moment of inertia matrix of the spacecraft is constant, because of the rigid body assumption. The first inertial time derivative of $\vec{\mathbf{h}}$ in the body-fixed reference frame is

$$\frac{\mathrm{d}^i}{\mathrm{d}t}\vec{\mathbf{h}}|_b = \dot{\mathbf{h}} + \boldsymbol{\omega}^{\times}\mathbf{h} \tag{3.23}$$

$$= \mathbf{I}\dot{\boldsymbol{\omega}} + \boldsymbol{\omega}^{\times}\mathbf{I}\boldsymbol{\omega} \tag{3.24}$$

Euler's equation states that[24]

$$\frac{\mathrm{d}\vec{\mathbf{h}}}{\mathrm{d}t} = \vec{\mathbf{g}} \tag{3.25}$$

where $\vec{\mathbf{g}}$ is the external torque acting on the spacecraft. A useful form of the equations of motion is found by combining Eqs. (3.24) and (3.25) and rearranging the terms to arrive at

$$\mathbf{I}\dot{\boldsymbol{\omega}} = \mathbf{g} - \boldsymbol{\omega}^{\times}\mathbf{I}\boldsymbol{\omega} \tag{3.26}$$

Equation (3.26) is the form of the equations of motion used in the development of the controllers presented in the next two chapters.

3.4 Attitude Error Dynamics

The development of the attitude controllers in the next chapter requires the definition of attitude kinematic error variables. There are two measures of attitude error of an individual spacecraft in a formation. The error measures are the station-keeping and formation-keeping attitude state errors.

3.4.1 Station-Keeping Error

Station-keeping error is the attitude state error of an individual spacecraft with respect to its absolute desired attitude. The station-keeping attitude error, $\delta\bar{\mathbf{q}}$, is defined

$$\delta\bar{\mathbf{q}} = \bar{\mathbf{q}} \otimes \hat{\bar{\mathbf{q}}}^{-1} \tag{3.27}$$

where $\hat{\bar{\mathbf{q}}}$ is the absolute desired attitude of the spacecraft formation. Using Eq. (3.20), the first time derivative of $\delta\bar{\mathbf{q}}$ is

$$\delta\dot{\bar{\mathbf{q}}} = \frac{1}{2}\delta\bar{\boldsymbol{\omega}} \otimes \delta\bar{\mathbf{q}} \tag{3.28}$$

The station-keeping angular velocity error, $\delta\boldsymbol{\omega}$, is defined as

$$\delta\boldsymbol{\omega} = \boldsymbol{\omega} - \mathbf{R}\left(\delta\bar{\mathbf{q}}\right)\hat{\boldsymbol{\omega}} \tag{3.29}$$

where $\hat{\boldsymbol{\omega}}$ is the absolute desired angular velocity vector expressed in the absolute desired reference frame. The first time derivative of $\delta\boldsymbol{\omega}$ is required in the development of the attitude tracking controller. It is defined as

$$\delta\dot{\boldsymbol{\omega}} = \dot{\boldsymbol{\omega}} - \mathbf{R}\left(\delta\bar{\mathbf{q}}\right)\dot{\hat{\boldsymbol{\omega}}} + \delta\boldsymbol{\omega}^{\times}\mathbf{R}\left(\delta\bar{\mathbf{q}}\right)\hat{\boldsymbol{\omega}} \tag{3.30}$$

where Eq. (3.9). The station-keeping error measure is used to determine the station-keeping behavior control action.

3.4.2 Formation-Keeping Error

Formation-keeping error is the attitude state error of the individual spacecraft with respect to the other spacecraft in the formation. The desired relative attitudes of the spacecraft in the formation are assumed to be constant. The formation-keeping attitude error presents a challenge if there are more than two spacecraft in the formation, because a physically relevant average attitude measure does not exist. The equations developed in this section deal with the error between two spacecraft in the formation. The attitude error between the jth and kth spacecraft, $\bar{\mathbf{q}}_{jk}$, is

$$\bar{\mathbf{q}}_{jk} = \bar{\mathbf{q}}_j \otimes \bar{\mathbf{q}}_k^{-1} \tag{3.31}$$

and can be defined in terms $\delta\bar{\mathbf{q}}_j$ and $\delta\bar{\mathbf{q}}_k$,

$$\begin{aligned}\bar{\mathbf{q}}_{jk} &= \delta\bar{\mathbf{q}}_j \otimes \hat{\bar{\mathbf{q}}}_j^{-1} \otimes \left(\delta\bar{\mathbf{q}}_k \otimes \hat{\bar{\mathbf{q}}}_k^{-1}\right)^{-1} \\ &= \delta\bar{\mathbf{q}}_j \otimes \hat{\bar{\mathbf{q}}}_j^{-1} \otimes \hat{\bar{\mathbf{q}}}_k \otimes \delta\bar{\mathbf{q}}_k^{-1} \\ &= \delta\bar{\mathbf{q}}_j \otimes \delta\bar{\mathbf{q}}_k^{-1}\end{aligned} \tag{3.32}$$

The time derivative of $\bar{\mathbf{q}}_{ij}$ is

$$\dot{\bar{\mathbf{q}}}_{jk} = \frac{1}{2}\bar{\boldsymbol{\omega}}_{jk} \otimes \bar{\mathbf{q}}_{jk} \tag{3.33}$$

where the relative angular velocity vector of the jth spacecraft with respect to the kth spacecraft, $\boldsymbol{\omega}_{jk}$, is defined as

$$\boldsymbol{\omega}_{jk} = \boldsymbol{\omega}_j - \mathbf{R}^{jk}\boldsymbol{\omega}_k \tag{3.34}$$

and can be defined in terms $\delta\boldsymbol{\omega}_j$ and $\delta\boldsymbol{\omega}_k$,

$$\begin{aligned}\boldsymbol{\omega}_{jk} &= \delta\boldsymbol{\omega}_j + \mathbf{R}\left(\delta\bar{\mathbf{q}}_j\right)\hat{\boldsymbol{\omega}} - \mathbf{R}^{jk}\left(\delta\boldsymbol{\omega}_k + \mathbf{R}\left(\delta\bar{\mathbf{q}}_k\right)\hat{\boldsymbol{\omega}}\right) \\ &= \delta\boldsymbol{\omega}_j - \mathbf{R}^{jk}\delta\boldsymbol{\omega}_k \end{aligned} \tag{3.35}$$

The control action for the formation-keeping behavior is determined using the formation-keeping error measures developed in this section.

3.5 Summary

A brief review of spacecraft attitude dynamics was given in this chapter. The important basic concepts of vectors, reference frames, and attitude were introduced and defined. The attitude representations used in this work were introduced and defined. The attitude kinematic and dynamic equations of motion were presented. Attitude error variables for the spacecraft formation attitude control problem were developed. The concepts and equations introduced in this chapter are used in the next chapter to develop control laws for a single, rigid spacecraft.

Chapter 4

Spacecraft Attitude Control

Nonlinear techniques for the analysis of the stability characteristics of a nonlinear controller are introduced in this chapter. Two attitude controllers for a single spacecraft are analyzed using these techniques. The analytic stability and convergence results are reinforced using numeric simulation results. The attitude controllers are extended in the next chapter to develop coordinated attitude controllers for a spacecraft formation.

4.1 Lyapunov Stability Theory

The goal of a controller is to determine the control actions required to ensure that the desired state or trajectory of the system is an asymptotically stable equilibrium point of the system. Techniques for the analysis of the stability of equilibrium points of autonomous systems are introduced in this section. A system whose dynamics are independent of time is an autonomous system. A general state-space representation of an autonomous system is

$$\dot{\mathbf{x}} = \mathbf{f}(\mathbf{x}) \tag{4.1}$$

An equilibrium point of the system, $\hat{\mathbf{x}}$, satisfies the equation,

$$\mathbf{f}(\hat{\mathbf{x}}) = \mathbf{0} \tag{4.2}$$

An equilibrium point is stable, in the sense of Lyapunov, if a solution that begins near the equilibrium point will stay near the equilibrium point for all time, otherwise the equilibrium

point is unstable.[26] A formal mathematical definition for the stability of an equilibrium point is presented in Definition 1.

Definition 1 (Stability of an Equilibrium Point[26]) An equilibrium point, $\hat{\mathbf{x}}$, of the system described by Eq. (4.1) is stable if and only if

$$\|\hat{\mathbf{x}} - \mathbf{x}(0)\| < \delta \quad \Rightarrow \quad \|\hat{\mathbf{x}} - \mathbf{x}(t)\| < \epsilon, \quad \forall \quad t \geq 0$$

where δ and ϵ are positive constants. □

An equilibrium point is asymptotically stable, if a solution that begins near the equilibrium point tends toward the equilibrium point as time progresses. Definition 2 presents a formal mathematical definition for the asymptotic stability of an equilibrium point.

Definition 2 (Asymptotic Stability of an Equilibrium Point[26]) An equilibrium point, $\hat{\mathbf{x}}$, of the system described by Eq. (4.1) is asymptotically stable if and only if

$$\|\hat{\mathbf{x}} - \mathbf{x}(0)\| < \delta \quad \Rightarrow \quad \lim \|\hat{\mathbf{x}} - \mathbf{x}(t)\| = \mathbf{0}, \quad \forall \quad t \geq 0$$

where δ is a positive constant. □

Lyapunov stability theory is useful in the analysis of nonlinear systems. Analytic solutions to nonlinear systems are often difficult to obtain. Lyapunov stability theory allows for the stability analysis of equilibrium points without determining analytic solutions to the nonlinear system. In Lyapunov stability theory, a scalar-valued, vector function of the system states, called a Lyapunov function, V, is used to determine the stability characteristics of the system. The requirements on the Lyapunov function to guarantee local stability and local asymptotic stability of the system are presented in Theorem 1.

Theorem 1 (Lyapunov Stability Theorem[26]) *Let $\mathbf{x} = \hat{\mathbf{x}}$ be an equilibrium point for the system described by Eq. (4.1). Let V be a continuously differentiable function on a neighborhood D of $\mathbf{x}$ that maps R^n on to R, such that*

$$V(\hat{\mathbf{x}}) = 0 \quad \textit{and} \quad V(\mathbf{x}) > 0 \quad \textit{in} \quad D - \{\hat{\mathbf{x}}\}$$

$$\dot{V}(\mathbf{x}) \leq 0 \quad \textit{in} \quad D$$

Then, $\mathbf{x} = \hat{\mathbf{x}}$ is a stable equilibrium point of the system. Moreover, if

$$\dot{V}(\mathbf{x}) < 0 \quad \textit{in} \quad D - \{\hat{\mathbf{x}}\}$$

Then, $\mathbf{x} = \hat{\mathbf{x}}$ is an asymptotically stable equilibrium point of the system. □

Global asymptotic stability of the system can be proven if the additional requirement of a radially-unbounded Lyapunov function is added to the asymptotic stability requirements presented in Theorem 1. Theorem 2 presents the formal mathematic requirements to prove global asymptotic stability of the system.

Theorem 2 (Barbashin-Krasovskii Theorem[26]) *Let* $\mathbf{x} = \hat{\mathbf{x}}$ *be an equilibrium point of the system described by Eq. (4.1). Let* V *be a continuously differentiable function of* $\mathbf{x}$ *that maps* R^n *on to* R*, such that*

$$V(\hat{\mathbf{x}}) = 0 \quad \textit{and} \quad V(\mathbf{x}) > 0, \quad \forall \quad \mathbf{x} \neq \hat{\mathbf{x}}$$

and, if

$$\|\mathbf{x}\| \to \infty \Rightarrow V(\mathbf{x}) \to \infty$$

$$\dot{V}(\mathbf{x}) < 0, \quad \forall \quad \mathbf{x} \neq \mathbf{0}$$

Then, $\mathbf{x} = \hat{\mathbf{x}}$ *is a globally asymptotically stable equilibrium point.* □

The analysis of the stability of spacecraft attitude controllers often leads to a negative-semi-definite $\dot{V}$. Therefore, only global stability can be proven using the theorems and definitions already given in the section. LaSalle's invariance principle provides a method to prove that the controller is asymptotically stable by investigating the solutions for which $\dot{V} = 0$. A formal statement of the invariance principle is presented in Theorem 3.

Theorem 3 (LaSalle's Invariance Principle[26]) *Let* $\mathbf{x} = \hat{\mathbf{x}}$ *be an equilibrium point of the system described by Eq. (4.1). Let* V *be a continuously-differentiable, radially-unbounded, positive-definite function of* $\mathbf{x}$ *that maps* R^n *on to* R*, such that* $\dot{V} \leq 0$ *for* $\mathbf{x} \in R^n$*. Let* S *be a subset of* R^n *where* $\dot{V} = 0$ *for* $\mathbf{x} \in S$*, and suppose that no solution can stay forever in* S *other than the solution at* $\hat{\mathbf{x}}$*. Then, the equilibrium point is globally asymptotically stable.* □

Stability definitions, Lyapunov stability theorems, and LaSalle's invariance principle were presented in this section. These definitions and theorems are used to prove the global asymptotic stability of the individual spacecraft attitude controllers presented in the next two sections.

4.2 Quaternion-Based Attitude Controller

A linear attitude control law for a single, rigid spacecraft using external control torques is

$$\mathbf{g} = -k_p\mathbf{q} - k_d\boldsymbol{\omega} \tag{4.3}$$

This control law was first introduced by Mortensen[27] and was later included in a survey of attitude representations for use in attitude control by Tsiotras.[28] The control law is proven to guarantee the attitude stability of a rigid body using the candidate Lyapunov function,

$$V = \frac{1}{2}\boldsymbol{\omega}^\mathsf{T}\mathbf{I}\boldsymbol{\omega} + k_p\mathbf{q}^\mathsf{T}\mathbf{q} + (1-q_4)^2 \tag{4.4}$$

Equation (4.4) defines a positive definite function that is radially unbounded. The first time derivative of V is

$$\dot{V} = \boldsymbol{\omega}^\mathsf{T}\mathbf{I}\dot{\boldsymbol{\omega}} + 2k_p\dot{\mathbf{q}}^\mathsf{T}\mathbf{q} - 2\left(1-q_4\right)\dot{q}_4 \tag{4.5}$$

Using Eq. (3.20), $\dot{V}$ simplifies to

$$\dot{V} = \boldsymbol{\omega}^\mathsf{T}\mathbf{I}\dot{\boldsymbol{\omega}} + k_p\boldsymbol{\omega}^\mathsf{T}\mathbf{q} \tag{4.6}$$

$$= \boldsymbol{\omega}^\mathsf{T}\left(\mathbf{I}\dot{\boldsymbol{\omega}} + k_p\mathbf{q}\right) \tag{4.7}$$

The closed-loop attitude dynamics of the spacecraft, Eqs. (3.26) and (4.3), are used to arrive at

$$\dot{V} = -k_d\boldsymbol{\omega}^\mathsf{T}\boldsymbol{\omega} \tag{4.8}$$

Equation (4.4) is a positive-definite, radially-unbounded function, whose first time derivative is negative semi-definite. Thus, V is a Lyapunov function, and the attitude of the spacecraft is globally stable, because the function satisfies the requirements of Theorem 1.

The convergence of the spacecraft's attitude is proven using an invariance argument. Equation (4.8) guarantees that

$$\lim_{t\to\infty}\boldsymbol{\omega} = \mathbf{0} \tag{4.9}$$

The closed-loop attitude dynamics of the spacecraft are

$$\mathbf{I}\dot{\boldsymbol{\omega}} = -k_p\mathbf{q} - k_d\boldsymbol{\omega} - \boldsymbol{\omega}^\times\mathbf{I}\boldsymbol{\omega} \tag{4.10}$$

Applying Eq. (4.9) to Eq. (4.10)

$$\mathbf{q} = \mathbf{0} \tag{4.11}$$

Therefore,

$$\lim_{t\to\infty} \mathbf{q} = \mathbf{0} \tag{4.12}$$

and the attitude of the spacecraft converges to the desired attitude.

4.2.1 Simulation Results

The stability analysis is reinforced by numeric simulation of a spacecraft using the quaternion-based attitude control law, Eq. (4.3). The moment of inertia matrix, $\mathbf{I}$, of the simulated spacecraft is

$$\mathbf{I} = \begin{bmatrix} 2 & 0 & 0 \\ 0 & 3 & 0 \\ 0 & 0 & 4 \end{bmatrix} \text{kg} \cdot \text{m}^2 \tag{4.13}$$

The control gains used for the simulation are

$$k_p = 3 \tag{4.14}$$

$$k_d = 5 \tag{4.15}$$

The control gains are chosen to allow the spacecraft to converge to the desired attitude in a reasonable time to prevent long simulation times. The ratio of the proportional and derivative gains was chosen to prevent severe oscillations of the spacecraft. Because, the stability and convergence results presented in the previous section are independent of the control gains, the actual values chosen for the gains are not critical. The attitude and angular velocity of the spacecraft are initialized to

$$\bar{\mathbf{q}}_0 = \begin{bmatrix} 0.0559 & 0.3652 & -0.0260 & 0.9289 \end{bmatrix}^\mathsf{T} \tag{4.16}$$

$$\boldsymbol{\omega}_0 = \begin{bmatrix} 0.0123 & -0.0123 & 0 \end{bmatrix}^\mathsf{T} \text{ rad/s} \tag{4.17}$$

The spacecraft is commanded to a desired attitude of

$$\hat{\bar{\mathbf{q}}} = \begin{bmatrix} 0 & 0 & 0 & 1 \end{bmatrix}^\mathsf{T} \tag{4.18}$$

which corresponds to with the inertial reference frame.

The results of the simulation are presented in Figures 4.1, 4.2, and 4.3. Figure 4.1 contains the angular error of the spacecraft, in degrees, throughout the simulation. Figure 4.2 contains plots of the angular rate error of the spacecraft in ^{o}/s. In both figures the upper plot displays the results using a linear scale and the lower plot uses a log scale on the ordinate axis. The semi-log plots are shown to better depict the features of the curves. The plots in both figures show that the spacecraft's attitude converges to the desired attitude. The angular error curve on the semi-log plot stops approximately 85 seconds into the simulation, because the error reaches "machine zero." The angular rate error decreases through the first 135 seconds of the simulation. After this point in the simulation the angular rate error has reached the integration tolerance limit, 10^{-8}.

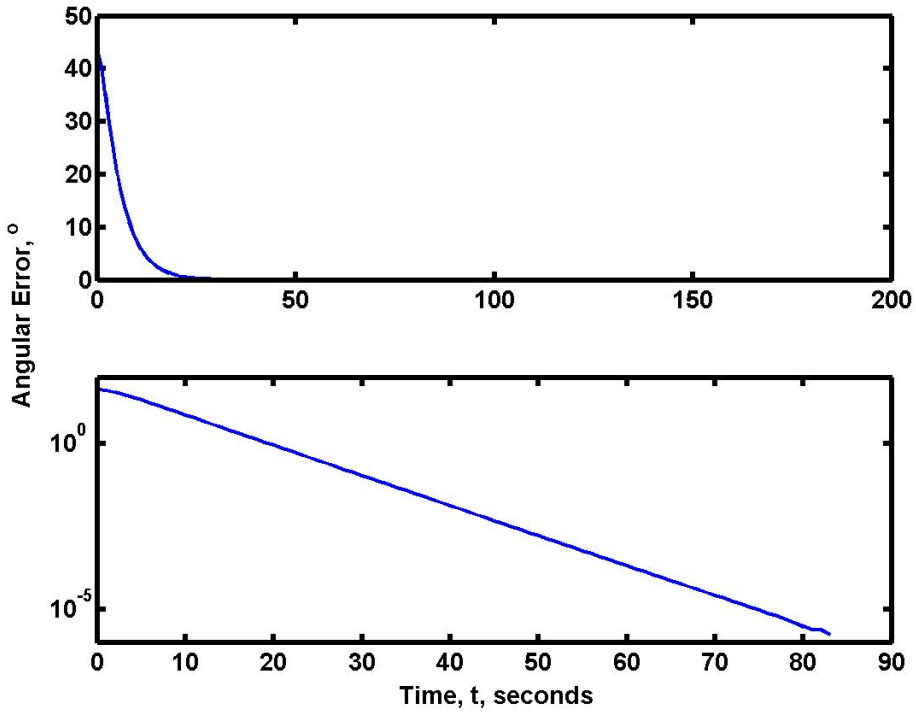

Figure 4.1: Angular error of the spacecraft during the simulation

Figure 4.3 is a plot of the magnitude of the control torque applied to the spacecraft throughout the simulation. As with the angular rate error curve the magnitude of the control torque reaches the integration tolerance limit approximately 135 seconds into the simulation.

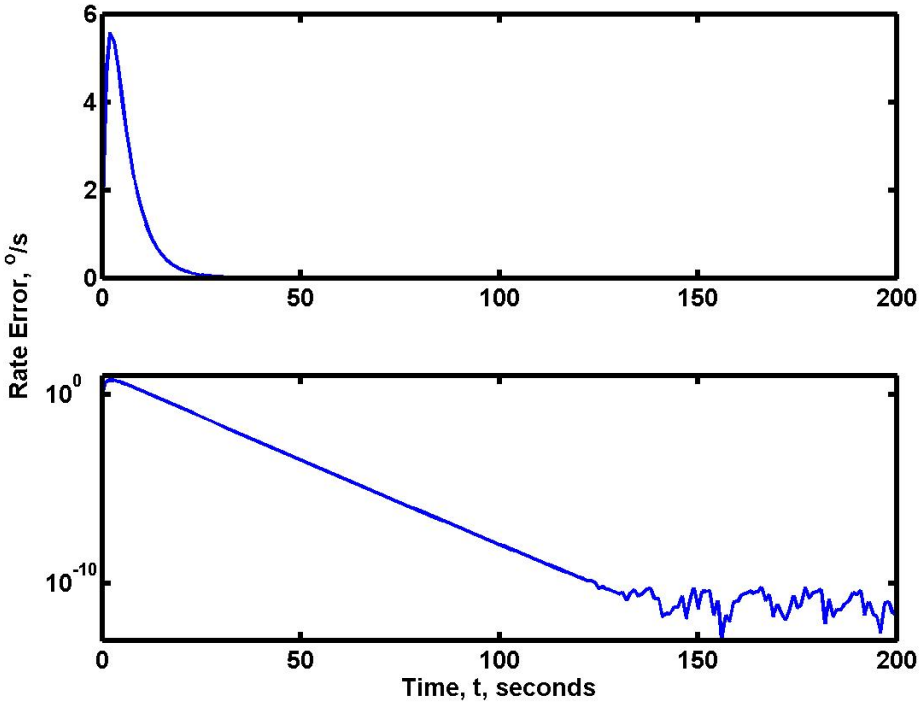

Figure 4.2: Angular rate error of the spacecraft during the simulation

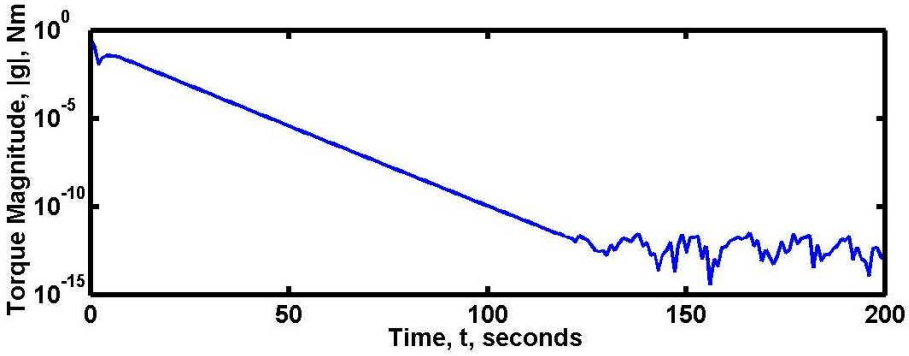

Figure 4.3: Magnitude of the control torque applied during the simulation

4.3 Quaternion-Based Attitude Tracking Controller

In this section, the quaternion-based attitude controller developed in the previous section is extended to provide trajectory tracking by using feedback linearization. A nonlinear attitude

tracking control law for a single, rigid spacecraft is

$$\mathbf{g} = \boldsymbol{\omega}^{\times}\mathbf{I}\boldsymbol{\omega} + \mathbf{I}\left(\mathbf{R}\left(\delta\mathbf{q}\right)\hat{\dot{\boldsymbol{\omega}}} + \delta\boldsymbol{\omega}^{\times}\mathbf{R}\left(\delta\mathbf{q}\right)\hat{\boldsymbol{\omega}}\right) - k_p\delta\mathbf{q} - k_d\delta\boldsymbol{\omega} \tag{4.19}$$

Equation (4.19) is an extended version of the control law presented in Eq. (4.3). The addition of the first two nonlinear terms in Eq. (4.19) allows the spacecraft to track a given reference attitude trajectory. The first term cancels out the nonlinear gyroscopic torque term in the rigid body equations of motion. The second term represents the control action required to follow the desired attitude trajectory.

The candidate Lyapunov function,

$$V = \frac{1}{2}\delta\boldsymbol{\omega}^{\mathsf{T}}\mathbf{I}\delta\boldsymbol{\omega} + k_p\delta\mathbf{q}^{\mathsf{T}}\delta\mathbf{q} + \left(1 - \delta q_4\right)^2 \tag{4.20}$$

is used to prove that the control law globally stabilizes the attitude of the spacecraft. Equation (4.20) is radially-unbounded and positive-definite. The first time derivative of the candidate Lyapunov function is

$$\dot{V} = \delta\boldsymbol{\omega}^{\mathsf{T}}\mathbf{I}\delta\dot{\boldsymbol{\omega}} + 2k_p\delta\dot{\mathbf{q}}^{\mathsf{T}}\delta\mathbf{q} - 2\left(1 - \delta q_4\right)\delta\dot{q}_4 \tag{4.21}$$

Using Eq. (3.20), $\dot{V}$ simplifies to

$$\dot{V} = \delta\boldsymbol{\omega}^{\mathsf{T}}\mathbf{I}\delta\dot{\boldsymbol{\omega}} + k_p\delta\boldsymbol{\omega}^{\mathsf{T}}\delta\mathbf{q} \tag{4.22}$$

$$= \delta\boldsymbol{\omega}^{\mathsf{T}}\left(\mathbf{I}\delta\dot{\boldsymbol{\omega}} + k_p\delta\mathbf{q}\right) \tag{4.23}$$

The equation is further simplified using the closed-loop attitude dynamics of the spacecraft,

$$\dot{V} = -k_d\delta\boldsymbol{\omega}^{\mathsf{T}}\delta\boldsymbol{\omega} \tag{4.24}$$

which is negative semi-definite. The candidate Lyapunov function, Eq. (4.19), is thus proven to be a true Lyapunov function. All of the conditions of Theorem 1 are satisfied, and therefore the quaternion-based attitude tracking control law globally stabilizes the spacecraft's attitude. The attitude tracking control law, Eq. (4.19), globally stabilizes the attitude of the spacecraft.

An invariance argument is used to prove that the attitude tracking control law guarantees global convergence of the spacecraft's attitude to the desired attitude reference trajectory. Equation (4.24) requires

$$\lim_{t\to\infty}\delta\boldsymbol{\omega} = \mathbf{0} \tag{4.25}$$

The closed-loop attitude dynamics of the spacecraft are

$$\mathbf{I}\delta\dot{\boldsymbol{\omega}} = -k_p\delta\mathbf{q} - k_d\delta\boldsymbol{\omega} \tag{4.26}$$

Applying Eq. (4.25) to Eq. (4.26)

$$\delta\mathbf{q} \;=\; \mathbf{0} \tag{4.27}$$

Therefore,

$$\lim_{t\to\infty}\delta\mathbf{q} \;=\; \mathbf{0} \tag{4.28}$$

The spacecraft's attitude converges to the desired attitude reference trajectory.

4.3.1 Simulation Results

Numeric simulation of a single spacecraft is performed to validate the analytic stability analysis presented for the quaternion-based attitude tracking controller, Eq. (4.19), in the previous section. The proportional and derivative control gains and the moment of inertia matrix used in the simulation are the same as those used in the quaternion-based attitude controller simulation. The attitude and angular velocity of the spacecraft are initialized to

$$\bar{\mathbf{q}}_0 \;=\; \begin{bmatrix} 0.1339 & 0.0529 & 0.0734 & 0.9869 \end{bmatrix}^{\mathsf{T}} \tag{4.29}$$

$$\boldsymbol{\omega}_0 \;=\; \begin{bmatrix} 0.0011 & 0.0745 & 0.0548 \end{bmatrix}^{\mathsf{T}} \text{ rad/s} \tag{4.30}$$

The spacecraft is commanded to track the attitude trajectory of a reference spacecraft that is performing a 90^o slew maneuver about its $\vec{\mathbf{b}}_2$ axis in 90 seconds. The initial attitude of the reference spacecraft is set to

$$\hat{\bar{\mathbf{q}}}_0 \;=\; \begin{bmatrix} 0 & 0 & 0 & 1 \end{bmatrix}^{\mathsf{T}} \tag{4.31}$$

The simulation results are presented in Figures 4.4, 4.5, and 4.6. Figure 4.4 contains the angular error of the spacecraft, in radians, throughout the simulation. Figure 4.5 contains plots of the angular rate error of the spacecraft in rad/s. In both figures the upper plot displays the results using a linear scale and the lower plot uses a log scale on the ordinate axis. The spacecraft's attitude converges to follow the desired attitude trajectory. The gaps

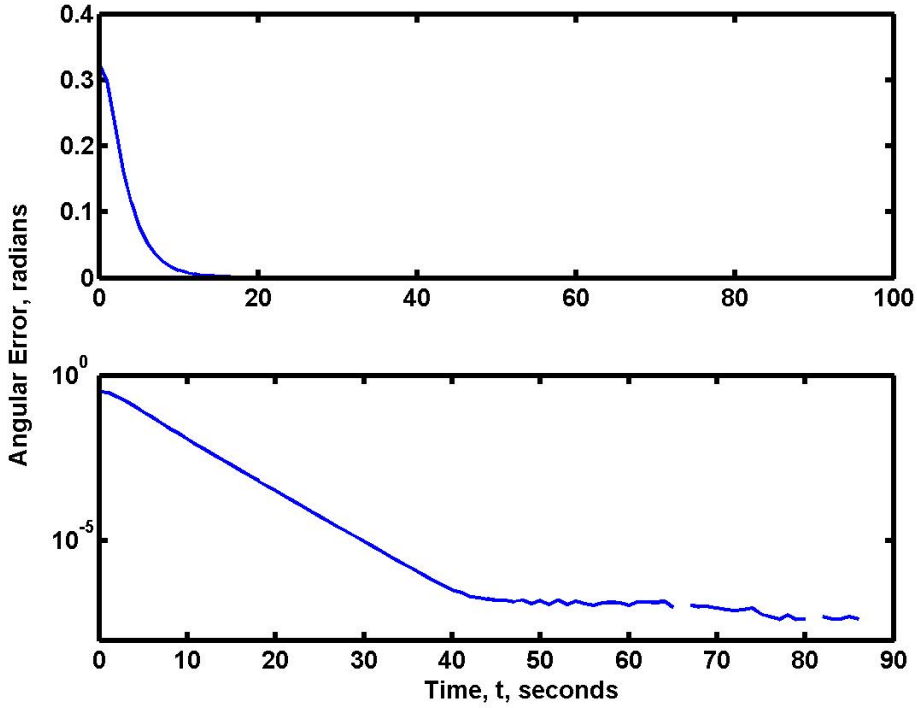

Figure 4.4: Angular error of the spacecraft tracking an attitude trajectory during the simulation

in the angular error curve occur because the error reaches "machine zero." The angular rate error decreases through the first 80 seconds of the simulation until the error has reached the integration tolerance limit.

A plot of the magnitude of the control torque applied to the spacecraft throughout the simulation is shown in Figure 4.6. The magnitude of the control torque reaches the integration tolerance limit near the end of the simulation, signifying the end of the slew maneuver.

4.4 Summary

Nonlinear attitude control of a single, rigid spacecraft was discussed in this chapter. A quaternion-based attitude controller and a quaternion-based attitude tracking controller were developed. Lyapunov stability theory and LaSalle's invariance principle were used to prove that the controllers guarantee the global convergence and stability of the spacecraft's

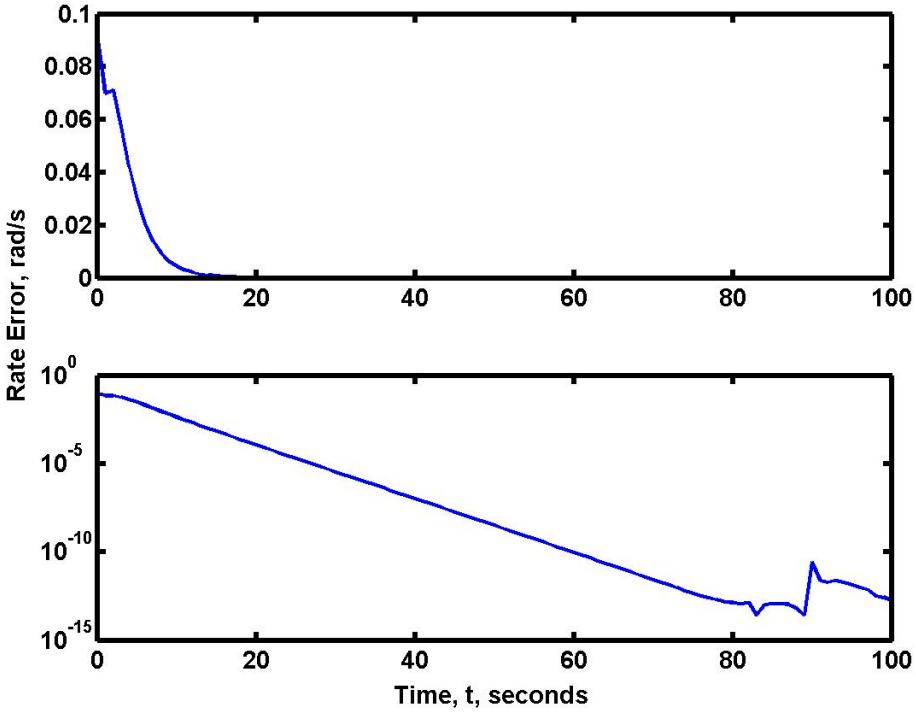

Figure 4.5: Angular rate error of the spacecraft tracking an attitude trajectory during the simulation

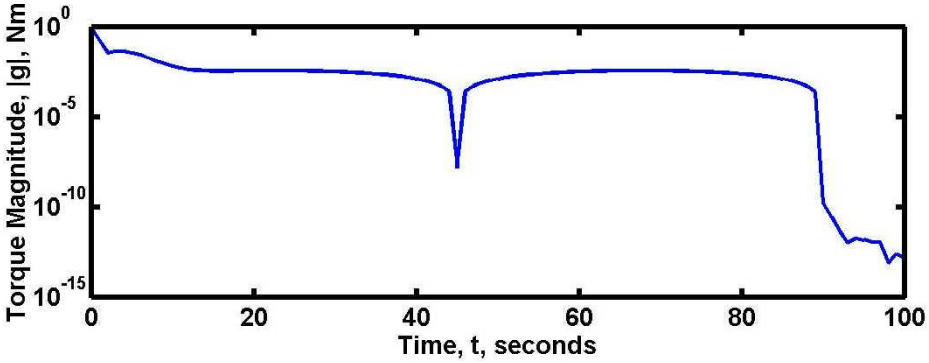

Figure 4.6: Magnitude of the control torque applied during the simulation of the spacecraft tracking an attitude trajectory

attitude. The analytic stability and convergence results were validated through numeric simulation. The attitude controllers presented in this chapter are extended in the next chapter for the development of coordinated attitude controllers for a spacecraft formation. The

analytic stability and convergence analysis methods introduced in this chapter are used to analyze the coordinated attitude controllers.

Chapter 5

Spacecraft Formation Attitude Control

The deficiencies in the literature discussed in Chapter 2 are resolved in this chapter. A class of decentralized attitude control laws is introduced. The control laws extend the quaternion-based attitude control law and the quaternion-based attitude tracking control law developed in the previous chapter. The analytical methods presented in Chapter 4 are used to prove that the class of control laws guarantee global stability and convergence of the spacecraft formation.

5.1 Problem Statement

The problem is formally defined before introducing the class of attitude control laws. The coordination of the attitude control systems of a spacecraft formation is considered. First, the approach used in solving the problem is discussed. Then the assumptions used in the development and analysis of the class of control laws are stated. Finally, the scope of the research is defined.

5.1.1 Approach

The two control methodology challenges presented by spacecraft formation attitude control are coordination and conflicting desired control behaviors.

The spacecraft formation is treated as a distributed system. The control systems of the individual spacecraft are coordinated through the communication of attitude state data. A decentralized coordination architecture is used, because of the system architecture benefits and the lack of prior proper investigation of this approach. Systems that use decentralized control architectures are fault-tolerant, and simple to upgrade and repair. Decentralized architectures are fault-tolerant because the resulting system does not have a single point of failure. Failure of a local subsystem does not lead to the destabilization of the entire system.[18] Repairs to the formation can simply be performed by replacing malfunctioning spacecraft. Upgrades can take the form of replacing obsolete spacecraft with a more advanced version, or by simply adding spacecraft to the formation. The drawback of decentralized controllers is the difficulty in producing analytic convergence proofs. The problem of analytic convergence proofs for decentralized controllers is discussed and resolved in this chapter.

Coordination is also accomplished through the use of the virtual structure method. The virtual structure method models the formation as one large, rigid spacecraft. The attitude of the virtual structure is the desired absolute attitude of the formation. Each spacecraft is able to determine its desired absolute attitude, because each spacecraft knows the attitude trajectory of the virtual structure and its constant attitude offset from that attitude. The addition of these rotations is the desired absolute attitude of the spacecraft.

An attitude control system of a spacecraft in a formation has two desired control behaviors: station-keeping and formation-keeping. The two behaviors often conflict due to the inevitable tracking errors of the spacecraft. Behavior-based control is used to reconcile the conflict and concurrently satisfy the desired control behaviors. The attitude control laws for the spacecraft in the formation are extended versions of the single spacecraft attitude control laws presented in the previous chapter. The single spacecraft attitude control laws represent the station-keeping behavior control terms. The formation-keeping behavior is satisfied by adding terms involving the relative attitude states of the spacecraft in the formation. The resultant control action is a compromise between the station-keeping and formation-keeping desired control behaviors.

Lyapunov stability theory is used to analyze the stability characteristics of the coordinated attitude control laws. A spacecraft formation is a special case of a distributed system where the subsystems are similar with respect to the form of their equations of motion. Therefore, it is prudent to separate the system's Lyapunov function into component Lyapunov functions for each subsystem. A component Lyapunov function incorporates all information about a specific subsystem (e.g. individual spacecraft). The Lyapunov function for the global system, the composite Lyapunov function, is the sum of the component Lyapunov functions. The composite Lyapunov function can be used to investigate the stability and convergence characteristics of the global system using Lyapunov stability theory. The stability characteristics of the coordinated attitude control laws are investigated using component and composite Lyapunov functions.[26]

5.1.2 Assumptions

Several assumptions relating to the nature of the spacecraft formation and the individual spacecraft are made to simplify the development and analysis of the class of decentralized attitude control laws. The spacecraft formation is assumed to have a rigid configuration and to be free-flying. The rigid configuration constraint requires that the desired relative attitudes of the spacecraft in the formation be constant. Therefore, the desired relative angular velocity of the spacecraft in the formation is identically zero. A free-flying spacecraft formation has no physical connections between the spacecraft in the formation, such as tethers or booms. The individual spacecraft interact only through the communication of state information between the spacecraft.

The spacecraft are assumed to be rigid bodies that use external torque actuation for attitude control. The rigid body assumption simplifies the attitude dynamics of the spacecraft. Although external torque actuation is used in developing the coordinated control laws, extending the results to use internal torque actuation is a straight-forward matter. The internal torque actuation extension is not included because there are no important or significant differences in that development.

5.1.3 Scope of Research

The focus of this research is the development of a decentralized coordinated attitude control law. An emphasis is placed on proving analytically that the decentralized controller guarantees a global asymptotically stable system. The effects of the control law parameters, such as control gains and coordination architecture are also investigated.

An in-depth analysis of the effects of communication disturbances between spacecraft and parameter uncertainties on the performance and stability of the spacecraft formation is not within the scope of this work. The communication between spacecraft is considered perfect. Each spacecraft knows its current attitude and the current attitudes of the spacecraft that are communicating with it at all times. Communication interrupts or failures are not considered. Bandwidth limitations on communication are also not considered. Uncertainty effects are not included in the scope of this research. The controllers are assumed to have perfect knowledge of the spacecraft parameters (e.g. moments of inertia). Control actuation is assumed to be perfect.

5.2 The Decentralized Coordinated Attitude Controller

As discussed in the Approach section, a behavior-based control methodology is used to develop the class of decentralized attitude control laws. The first step in behavior-based control is the determination of the control actions for the desired control behaviors.

5.2.1 Desired Behavior Control Actions

The two desired behaviors for a spacecraft formation are station-keeping and formation-keeping. The control action for the attitude-tracking station-keeping behavior for the jth spacecraft, $\mathbf{g}_j^s$, is calculated using

$$\mathbf{g}_j^s = \boldsymbol{\omega}_j^{\times}\mathbf{I}_j\boldsymbol{\omega}_j + \mathbf{I}_j\left(\mathbf{R}\left(\delta\bar{\mathbf{q}}_j\right)\dot{\hat{\boldsymbol{\omega}}} - \delta\boldsymbol{\omega}_j^{\times}\mathbf{R}\left(\delta\bar{\mathbf{q}}_j\right)\hat{\boldsymbol{\omega}}\right) - k_{p_j}\delta\mathbf{q}_j - k_{d_j}\delta\boldsymbol{\omega}_j \tag{5.1}$$

If the desired attitude of the formation is constant, then the station-keeping control action can be simplified to

$$\mathbf{g}_j^s = -k_{p_j}\mathbf{q}_j - k_{d_j}\boldsymbol{\omega}_j \tag{5.2}$$

Equations (5.1) and (5.2) are identical to the single spacecraft attitude control law, Eq. (4.3), and the single, spacecraft attitude tracking control law, Eq. (4.19), presented in Chapter 4. The station-keeping control action drives the absolute attitude state error to zero.

The control action for the formation-keeping behavior for the jth spacecraft, $\mathbf{g}_j^f$, is calculated using

$$\mathbf{g}_j^f = -\sum_{k=1}^{n} \rho_{jk}^p \mathbf{q}_{jk} - \sum_{k=1}^{n} \rho_{jk}^d \boldsymbol{\omega}_{jk} \tag{5.3}$$

where ρ_{jk}^p is the proportional formation-keeping behavior weighting, ρ_{jk}^d is the derivative formation-keeping behavior weighting, and n is the number of spacecraft in the formation. The control action for the formation-keeping behavior drives the relative attitude state error, $\mathbf{q}_{jk}$ and $\boldsymbol{\omega}_{jk}$, between connected spacecraft to zero. The proportional behavior weighting factor, ρ_{jk}^p, determines the importance of the relative alignment of the jth and the kth spacecraft in the formation. The derivative behavior weighting factor, ρ_{jk}^d, determines the importance of the jth and the kth spacecraft in the formation maintaining the same angular rate. The value of ρ_{jk}^p is restricted so that

$$\rho_{jk}^p \geq 0 \text{ and } \sum_{k=1}^{n} \rho_{jk}^p < k_{p_j} \quad \forall \; j = 1, 2, ..., n \tag{5.4}$$

and the value of ρ_{jk}^d is restricted so that

$$\rho_{jk}^d \geq 0 \tag{5.5}$$

These restrictions are necessary for the convergence proof presented later in this chapter. Both the proportional and derivative behavior weights are further restricted by

$$\rho_{jk} = \rho_{kj} \tag{5.6}$$

The second restriction, Eq. (5.6), requires that the importance of the relative alignment and angular rate of the jth and kth spacecraft be the same for the jth spacecraft and the kth spacecraft.

5.2.2 The Control Law

The decentralized attitude control law is determined by summing the control actions for the station-keeping and formation-keeping behaviors. The resulting control law for the jth

spacecraft, $\mathbf{g}_j$, is

$$\begin{aligned} \mathbf{g}_j &= \mathbf{g}_j^s + \mathbf{g}_j^f \\ &= \boldsymbol{\omega}_j^{\times}\mathbf{I}_j\boldsymbol{\omega}_j + \mathbf{I}_j\left(\mathbf{R}\left(\delta\bar{\mathbf{q}}_j\right)\dot{\hat{\boldsymbol{\omega}}} - \delta\boldsymbol{\omega}_j^{\times}\mathbf{R}\left(\delta\bar{\mathbf{q}}_j\right)\hat{\boldsymbol{\omega}}\right) - k_p\delta\mathbf{q}_j - k_d\delta\boldsymbol{\omega}_j \\ &\quad - \sum_{k=1}^{n}\rho_{jk}^p\mathbf{q}_{jk} - \sum_{k=1}^{n}\rho_{jk}^d\boldsymbol{\omega}_{jk} \end{aligned} \tag{5.7}$$

The control law, Eq. (5.7), is an extension of the single spacecraft quaternion-based attitude tracking control law presented in Chapter 4. The control law is extended in recognition that the spacecraft is part of a larger system, the spacecraft formation. The two summation terms appended to the end of the equation represent the modification. These terms enforce an interconnection between the spacecraft in the formation. Throughout the rest of this work, a non-zero ρ_{jk} is referred to as a connection between spacecraft. The magnitude of ρ_{jk} represents the strength of the connection between the spacecraft. This terminology is used to more clearly indicate the interdependency of the spacecraft in the formation.

5.3 Coordination Architectures

Equation (5.7) represents a class of decentralized control laws that differ by the coordination architecture used by the spacecraft formation. The choice of the formation-keeping weighting factors, ρ_{jk}, determine the coordination architecture used. Variants of coordination architectures can be created by altering the number of connections between spacecraft and the strength of the connections.

Four different coordination architectures for a six-spacecraft formation are presented in Figure 5.1. The circles represent the individual spacecraft. Connections between the spacecraft are denoted by bi-directional arrows. The coordination architectures in Figure 5.1 differ in the number of connections per spacecraft, c, used. Diagram A depicts an architecture with no connection between the spacecraft. In this architecture the spacecraft act independently as if they were not part of a formation. Diagram B shows a coordination architecture with two connections per spacecraft. This type of coordination architecture is used by the velocity feedback controller presented in Lawton and Beard[14] and the "coupled-dynamics controller" presented in Lawton, Beard and Hadaegh.[10] The authors term the two-connection architecture the "ring" coordination architecture. Diagram C shows an architecture with three

connections per spacecraft. A coordination architecture where each spacecraft is connected to four other spacecraft in the formation is displayed in Diagram D. The addition of one more connection per spacecraft would create a fully-connected architecture, where each spacecraft is connected to every other spacecraft in the formation.

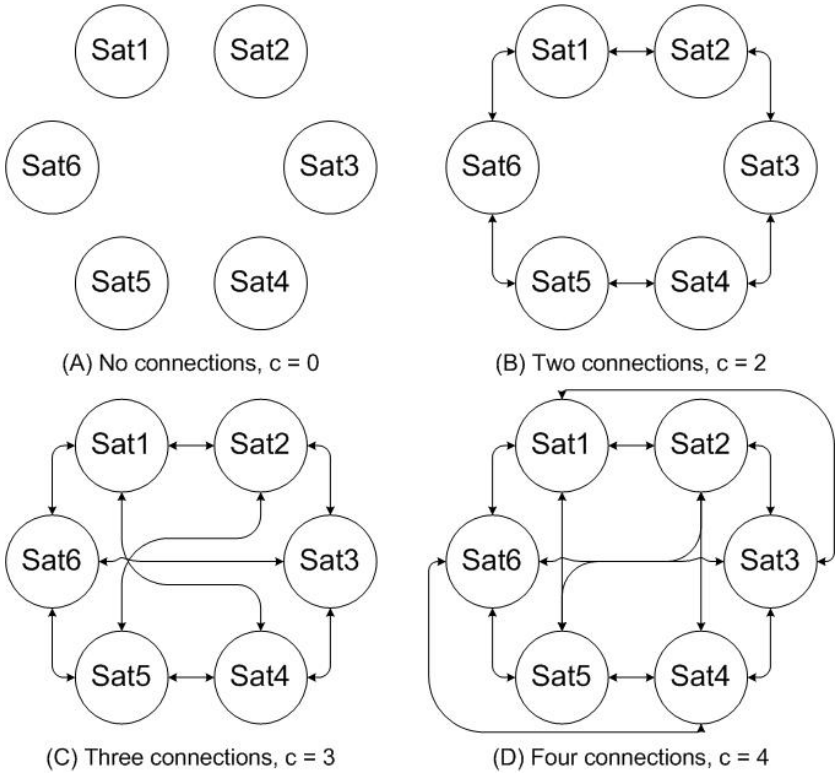

Figure 5.1: Four decentralized coordination architectures using a different number of connections between spacecraft in the formation

The spacecraft in the formation are not constrained to have the same number of connections. Figure 5.2 is a diagram of a simple three-spacecraft coordination architecture where the spacecraft in the formation do not all have the same number of connections. Sat 1 has two connections, while Sats 2 and 3 have only one connection.

Coordination architectures can differ by altering the weights of the connections. An example diagram of a spacecraft using connections with different weights is presented in Figure 5.3. The spacecraft is connected to four other spacecraft in the formation. The connections are represented by the arrows directed away from the Sat. The width of the arrows depicts the relative strength of the connections. For example, Connection 1 is stronger than Connections

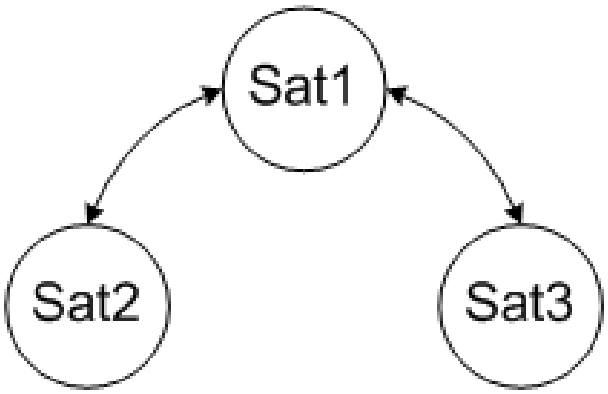

Figure 5.2: A coordination architecture where the individual spacecraft do not all have the same number of connections

2, 3, and 4. The connection strengths show that it is most important for the Sat to be aligned with the spacecraft connected to it through Connection 1.

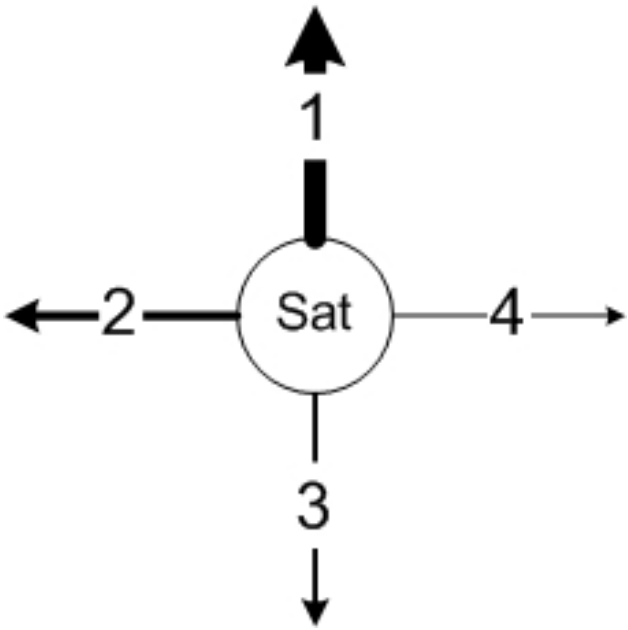

Figure 5.3: A spacecraft that is connected to four other spacecraft in the formation using different weights

One interesting coordination scheme involves grouping the spacecraft in a formation into clusters of strongly connected spacecraft. The clusters are then lightly connected through connections between spacecraft in different clusters. Figure 5.4 shows a nine-spacecraft

coordination architecture that makes use of clusters. The nine spacecraft are grouped in to three clusters of three spacecraft each. The clusters are denoted by the red, green, and blue circles around the three spacecraft. The strong connections within the clusters are represented by the solid bi-directional arrows. The weak connections between spacecraft in different clusters are denoted by the dotted bi-directional arrows.

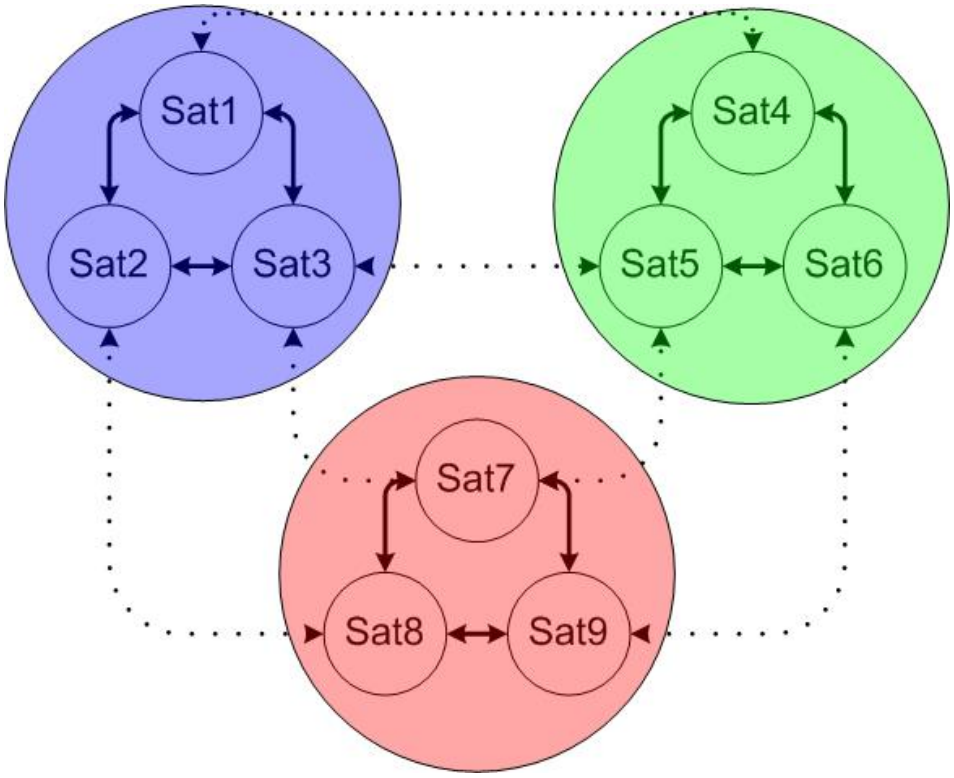

Figure 5.4: A decentralized coordination architecture that groups spacecraft into clusters

The few coordination architectures presented in this section represent only a small sampling of the possible architectures. The choice of coordination architecture is limited only by the imagination and ingenuity of the system designer.

5.4 Global Stability and Convergence Proofs

The class of decentralized attitude control laws is proven to globally stabilize the system using the convergence and stability theorems presented in Chapter 4. First, Lyapunov stability

theory is used to prove that the system is globally stable. The component Lyapunov function for the jth spacecraft is

$$\begin{aligned} V_j &= \frac{1}{2}\delta\boldsymbol{\omega}_j^{\mathsf{T}}\mathbf{I}_j\delta\boldsymbol{\omega}_j + k_{p_j}\delta\mathbf{q}_j^{\mathsf{T}}\delta\mathbf{q}_j + k_{p_j}(1-\delta q_{j,4})^2 \\ &\quad + \frac{1}{2}\sum_{k=1}^{n}\rho_{jk}^{p}\left(\mathbf{q}_{jk}^{\mathsf{T}}\mathbf{q}_{jk} + (1-q_{jk,4})^2\right) \end{aligned} \tag{5.8}$$

which is a positive-definite, radially-unbounded function. The composite Lyapunov function for the spacecraft formation is formed by summing all of the component Lyapunov functions.

$$V = \sum_{j=1}^{n} V_j \tag{5.9}$$

The first time derivative of the composite Lyapunov function is simply

$$\dot{V} = \sum_{j=1}^{n} \dot{V}_j \tag{5.10}$$

The first time derivative of the component Lyapunov function is

$$\begin{aligned} \dot{V}_j &= \delta\boldsymbol{\omega}_j^{\mathsf{T}}\mathbf{I}_j\delta\dot{\boldsymbol{\omega}}_j + 2k_{p_j}\delta\dot{\mathbf{q}}_j^{\mathsf{T}}\delta\mathbf{q}_j - 2k_{p_j}(1-\delta q_j^4)\delta\dot{q}_{j,4} \\ &\quad + \frac{1}{2}\sum_{k=1}^{n}\rho_{jk}^{p}\left(2\dot{\mathbf{q}}_{jk}^{\mathsf{T}}\mathbf{q}_{jk} - 2k_p(1-q_{jk}^4)\dot{q}_{jk,4}\right) \end{aligned} \tag{5.11}$$

$$= \delta\boldsymbol{\omega}_j^{\mathsf{T}}\mathbf{I}_j\delta\dot{\boldsymbol{\omega}}_j + k_{p_j}\delta\boldsymbol{\omega}_j^{\mathsf{T}}\delta\mathbf{q}_j + \frac{1}{2}\sum_{k=1}^{n}\rho_{jk}^{p}\boldsymbol{\omega}_{jk}^{\mathsf{T}}\mathbf{q}_{jk} \tag{5.12}$$

$$= \delta\boldsymbol{\omega}_j^{\mathsf{T}}\left(\mathbf{I}_j\delta\dot{\boldsymbol{\omega}}_j + k_{p_j}\delta\mathbf{q}_j\right) + \frac{1}{2}\sum_{k=1}^{n}\rho_{jk}^{p}\boldsymbol{\omega}_{jk}^{\mathsf{T}}\mathbf{q}_{jk} \tag{5.13}$$

The closed-loop attitude dynamics of the jth spacecraft are used in conjunction with Eq. (5.13) to arrive at

$$\dot{V}_j = -k_{d_j}\delta\boldsymbol{\omega}_j^{\mathsf{T}}\delta\boldsymbol{\omega}_j - \delta\boldsymbol{\omega}_j^{\mathsf{T}}\sum_{k=1}^{n}\rho_{jk}^{d}\boldsymbol{\omega}_{jk} - \delta\boldsymbol{\omega}_j^{\mathsf{T}}\sum_{k=1}^{n}\rho_{jk}^{p}\mathbf{q}_{jk} + \frac{1}{2}\sum_{k=1}^{n}\rho_{jk}^{p}\boldsymbol{\omega}_{jk}^{\mathsf{T}}\mathbf{q}_{jk} \tag{5.14}$$

The goal is to prove that the first time derivative of the Lyapunov function is negative definite. The first term of Eq. (5.14) is negative definite; however the sum of the last three terms is indefinite. Therefore, the component Lyapunov function is not a true Lyapunov function and no knowledge as to the stability of the individual spacecraft can be garnered.

The spacecraft formation can be proven to be stable if the sum of the component Lyapunov functions results in a negative definite function. The composite Lyapunov function is

$$\dot{V} = -\sum_{j=1}^{n} k_{d_j} \delta\boldsymbol{\omega}_j^{\mathsf{T}} \delta\boldsymbol{\omega}_j - \sum_{j=1}^{n} \left(\delta\boldsymbol{\omega}_j^{\mathsf{T}} \sum_{k=1}^{n} \rho_{jk}^{d} \boldsymbol{\omega}_{jk} - \delta\boldsymbol{\omega}_j^{\mathsf{T}} \sum_{k=1}^{n} \rho_{jk}^{p} \mathbf{q}_{jk} + \frac{1}{2} \sum_{k=1}^{n} \rho_{jk}^{p} \boldsymbol{\omega}_{jk}^{\mathsf{T}} \right) \mathbf{q}_{jk} \tag{5.15}$$

Summing the terms involving the relative attitude variables of the jth and kth spacecraft results in

$$\begin{aligned} -\rho_{jk}^{d} \delta\boldsymbol{\omega}_j^{\mathsf{T}} \boldsymbol{\omega}_{jk} - \rho_{kj}^{d} \delta\boldsymbol{\omega}_k^{\mathsf{T}} \boldsymbol{\omega}_{kj} &- \rho_{jk}^{p} \delta\boldsymbol{\omega}_j^{\mathsf{T}} \mathbf{q}_{jk} - \rho_{kj}^{p} \delta\boldsymbol{\omega}_k^{\mathsf{T}} \mathbf{q}_{kj} \\ +\frac{1}{2} \rho_{jk}^{p} \boldsymbol{\omega}_{jk}^{\mathsf{T}} \mathbf{q}_{jk} &+ \frac{1}{2} \rho_{kj}^{p} \boldsymbol{\omega}_{kj}^{\mathsf{T}} \mathbf{q}_{kj} \end{aligned} \tag{5.16}$$

The relation between the relative attitude kinematics of the spacecraft is

$$\boldsymbol{\omega}_{kj} = -\mathbf{R}^{kj} \boldsymbol{\omega}_{jk} \tag{5.17}$$

$$\mathbf{q}_{kj} = -\mathbf{q}_{jk} = -\mathbf{R}^{kj} \mathbf{q}_{jk} \tag{5.18}$$

Using these relations in Eq. (5.16) leads to

$$-\rho_{jk}^{d} \left(\delta\boldsymbol{\omega}_j - \mathbf{R}^{jk} \delta\boldsymbol{\omega}_k \right)^{\mathsf{T}} \boldsymbol{\omega}_{jk} - \rho_{jk}^{p} \left(\delta\boldsymbol{\omega}_j - \mathbf{R}^{jk} \delta\boldsymbol{\omega}_k \right)^{\mathsf{T}} \mathbf{q}_{jk} + \rho_{jk}^{p} \boldsymbol{\omega}_{jk}^{\mathsf{T}} \mathbf{q}_{jk} \tag{5.19}$$

The definition of the relative angular velocity vector, Eq. (3.35), is used to further simplify the equation to

$$-\rho_{jk}^{d} \boldsymbol{\omega}_{jk}^{\mathsf{T}} \boldsymbol{\omega}_{jk} \tag{5.20}$$

which is a negative definite quantity. If this process is performed for each connection, $\dot{V}$ is simplified to

$$\dot{V} = -\sum_{j=1}^{n} k_{d_j} \delta\boldsymbol{\omega}_j^{\mathsf{T}} \delta\boldsymbol{\omega}_j - \sum_{j=1}^{n} \sum_{k=j+1}^{n} \rho_{jk}^{d} \boldsymbol{\omega}_{jk}^{\mathsf{T}} \boldsymbol{\omega}_{jk} \tag{5.21}$$

which is negative definite. Thus, the candidate composite Lyapunov function is shown to be a true Lyapunov function, thereby proving the spacecraft formation is globally stable.

It must now be demonstrated that the decentralized controller presented earlier guarantees global convergence of the spacecraft formation's attitude. Equation (5.21) requires that

$$\lim_{t \to \infty} \delta\boldsymbol{\omega}_j = \lim_{t \to \infty} \boldsymbol{\omega}_{jk} = \mathbf{0} \tag{5.22}$$

If this result is applied to the closed-loop dynamics of the system, the result is a system of n equations of the form,

$$k_{p_j}\delta\mathbf{q}_j + \sum_{k=1}^{n}\rho_{jk}^{p}\mathbf{q}_{jk} = \mathbf{0} \tag{5.23}$$

Using the definition of $\bar{\mathbf{q}}_{jk}$, Eq. (5.23) can be re-written as

$$\begin{aligned}\mathbf{0} &= k_{p_j}\delta\mathbf{q}_j + \sum_{k=1}^{n}\rho_{jk}^{p}\left(\left(\delta\mathbf{q}_k^{\times} + \delta q_{k,4}\mathbf{1}\right)\delta\mathbf{q}_j - \delta q_{j,4}\delta\mathbf{q}_k\right) &(5.24)\\ &= k_{p_j}\delta\mathbf{q}_j + \left(\left(\sum_{k=1}^{n}\rho_{jk}^{p}\delta\mathbf{q}_k\right)^{\times} + \sum_{k=1}^{n}\rho_{jk}^{p}\delta q_{k,4}\mathbf{1}\right)\delta\mathbf{q}_j - \delta q_{j,4}\sum_{k=1}^{n}\rho_{jk}^{p}\delta\mathbf{q}_k &(5.25)\end{aligned}$$

which can be written in the convenient form,

$$\delta\mathbf{q}_j^{\times}\sum_{k=1}^{n}\rho_{jk}^{p}\delta\mathbf{q}_k = \left(k_{p_j} + \sum_{k=1}^{n}\rho_{jk}^{p}\delta q_{k,4}\right)\delta\mathbf{q}_j - \delta q_{kj,4}\sum_{k=1}^{n}\rho_{jk}^{p}\delta\mathbf{q}_k \tag{5.26}$$

The right side of Eq. (5.26) is a linear combination of the vectors, $\delta\mathbf{q}_j$ and $\sum_{k=1}^{n}\rho_{jk}^{p}\delta\mathbf{q}_k$, and the left side of the equation is the cross product of the same two vectors. The equality is only satisfied if

$$\delta\mathbf{q}_j^{\times}\sum_{k=1}^{n}\rho_{jk}^{p}\delta\mathbf{q}_k = \mathbf{0} \tag{5.27}$$

Therefore, Eq. (5.26) simplifies to

$$\left(k_{p_j} + \sum_{k=1}^{n}\rho_{jk}^{p}\delta q_{k,4}\right)\delta\mathbf{q}_j - \delta q_{j,4}\sum_{k=1}^{n}\rho_{jk}^{p}\delta\mathbf{q}_k = \mathbf{0} \tag{5.28}$$

which is solved for $\delta\mathbf{q}_j$

$$\delta\mathbf{q}_j = \frac{\delta q_{j,4}}{k_p + \sum_{k=1}^{n}\rho_{jk}^{p}\delta q_{k,4}}\sum_{k=1}^{n}\rho_{jk}^{p}\delta\mathbf{q}_k \tag{5.29}$$

The set of n equations that result can be represented in matrix form as

$$\mathbf{Q} = \mathbf{M}\mathbf{Q} \tag{5.30}$$

where the $3n \times 1$ column vector $\mathbf{Q}$

$$\mathbf{Q} = \begin{bmatrix}\delta\mathbf{q}_1^{\mathsf{T}} & \cdots & \delta\mathbf{q}_n^{\mathsf{T}}\end{bmatrix}^{\mathsf{T}} \tag{5.31}$$

The $3n \times 3n$ matrix $\mathbf{M}$ is defined

$$m_{jk} = \kappa_j \rho_{jk}^p \tag{5.32}$$

where

$$\kappa_j = \frac{\delta q_{j,4}}{k_{p_j} + \sum_{k=1}^{n} \rho_{jk}^p \delta q_{k,4}} \tag{5.33}$$

The upper limit of the magnitude of κ_j is

$$\kappa_j \leq \frac{1}{k_{p_j}} \tag{5.34}$$

This value becomes important later in the proof. Re-writing Eq. (5.30) in homogeneous form results in

$$(\mathbf{1} - \mathbf{M})\,\mathbf{Q} = \tilde{\mathbf{M}}\mathbf{Q} = \mathbf{0} \tag{5.35}$$

The equation can be satisfied if

$$\mathbf{Q} = \mathbf{0} \tag{5.36}$$

In order to prove that the formation will converge, Eq. (5.36), the matrix $\tilde{\mathbf{M}}$ is investigated. In block-matrix form, $\tilde{\mathbf{M}}$ is

$$\tilde{\mathbf{M}} = \begin{bmatrix} \mathbf{1} & -\kappa_1\rho_{12}^p\mathbf{1} & \cdots & -\kappa_1\rho_{1n}^p\mathbf{1} \\ -\kappa_2\rho_{21}^p\mathbf{1} & \ddots & \cdots & \vdots \\ \vdots & \cdots & \ddots & -\kappa_{n-1}\rho_{n-1|n}^p\mathbf{1} \\ -\kappa_n\rho_{n1}^p\mathbf{1} & \cdots & -\kappa_n\rho_{n|n-1}^p\mathbf{1} & \mathbf{1} \end{bmatrix} \tag{5.37}$$

The diagonal elements of the matrix are all 1. The sum of the off-diagonal elements of the jth row is

$$\sum_{k=1}^{n} -\kappa_j \rho_{jk}^p \tag{5.38}$$

and because of the restrictions on ρ_{jk}^p and upper magnitude limit of κ_j,

$$\left| \sum_{k=1}^{n} \kappa_j \rho_{jk}^p \right| < 1 \quad \forall\, j = 1, 2, ..., n \tag{5.39}$$

Therefore, $\tilde{\mathbf{M}}$ is a strictly diagonally dominant matrix and

$$\det\left(\tilde{\mathbf{M}}\right) \neq 0 \tag{5.40}$$

which means that the $\tilde{\mathbf{M}}$ is an invertible matrix.[29] The homogeneous equation, Eq. (5.35), can be solved for $\mathbf{Q}$ to arrive at

$$\mathbf{Q} = \tilde{\mathbf{M}}^{-1}\mathbf{0} = \mathbf{0} \tag{5.41}$$

Therefore, the only valid, stable equilibrium condition of the spacecraft formation is Eq. (5.36). The decentralized attitude control law thereby guarantees that the spacecraft formation will converge to the commanded desired attitude trajectory. The origin of the system can be shifted to allow the spacecraft formation to attain any attitude trajectory in any rigid configuration.

5.5 Summary

A class of decentralized attitude control laws was developed in this chapter. Coordination architectures that are possible with this class of control laws were discussed. The control laws were proven through analytic analysis to guarantee the global stability and convergence of the spacecraft formation. The next chapter further investigates the stability characteristics the class of control laws through numeric simulation.

Chapter 6

Simulation Results

The performance and stability characteristics of the class of decentralized attitude control laws developed in the previous chapter are investigated through numeric simulation. The stability analysis presented in the previous chapter is reinforced using a simulation of a spacecraft formation with no un-modelled effects. The performance of different coordination architectures is investigated using simulations including un-modelled disturbance torques.

6.1 Common Simulation Parameters

Investigating the performance of different coordination architectures requires that some simulation parameters not dealing with coordination architecture be held constant in the simulations. By holding these non-critical parameters constant meaningful comparisons can be made between simulations. Parameters common to the simulations presented in this chapter are defined in this section.

The simulations presented in this chapter are performed with an integration tolerance of 10^{-8}. The spacecraft formation's attitude is assumed to have converged to the desired attitude when the angular error reaches the integration tolerance. The spacecraft formation simulations require the definition of the reference spacecraft's attitude trajectory. The reference spacecraft performs a 180^o slew maneuver about its $\vec{\mathbf{b}}_2$ axis. The maneuver is completed

in 90 seconds. The initial attitude state of the reference spacecraft is

$$\hat{\bar{\mathbf{q}}}(t_0) = \begin{bmatrix} 0 & 0 & 0 & 1 \end{bmatrix}^{\mathsf{T}} \tag{6.1}$$

$$\hat{\boldsymbol{\omega}}(t_0) = \begin{bmatrix} 0 & 0 & 0 \end{bmatrix}^{\mathsf{T}} \text{ rad/s} \tag{6.2}$$

The attitude state of the reference spacecraft after the slew maneuver is

$$\hat{\bar{\mathbf{q}}}(t_f) = \begin{bmatrix} 0 & 1 & 0 & 0 \end{bmatrix}^{\mathsf{T}} \tag{6.3}$$

$$\hat{\boldsymbol{\omega}}(t_f) = \begin{bmatrix} 0 & 0 & 0 \end{bmatrix}^{\mathsf{T}} \text{ rad/s} \tag{6.4}$$

Figure 6.1 shows the time variation of the attitude state throughout the slew maneuver. The top plot shows the variation of the components of the quaternion. The change in the angular velocity vector components is shown in the bottom plot.

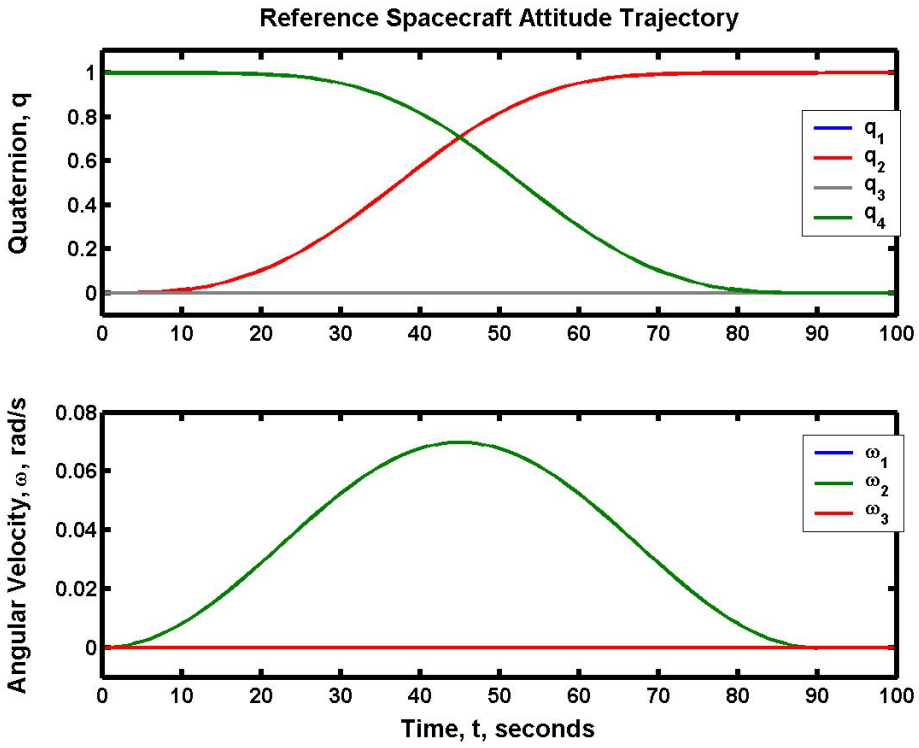

Figure 6.1: Attitude trajectory of the reference spacecraft

The individual spacecraft in the formation are assumed to be identical in the simulations.

The spacecraft are modelled as rigid bodies with a moment of inertia matrix of

$$\mathbf{I} = \begin{bmatrix} 2 & 0 & 0 \\ 0 & 3 & 0 \\ 0 & 0 & 4 \end{bmatrix} \text{ kg} \cdot \text{m}^2 \tag{6.5}$$

Because the spacecraft have identical moments of inertia, the station-keeping control gains are held constant. The proportional and derivative control gains used in the simulations are

$$k_p = 3 \tag{6.6}$$
$$k_d = 5 \tag{6.7}$$

The same initial attitude states of the spacecraft in the formation are used in each simulation. By using the same initial attitude states, direct performance comparisons between simulations can be appropriately performed. The initial attitude states of the spacecraft are presented in the Table 6.1. The numeric subscripts denote the corresponding spacecraft (e.g. $\boldsymbol{\omega}_6$ = angular velocity vector of the sixth spacecraft).

Table 6.1: Initial attitude states of the spacecraft in the formation

$\bar{\mathbf{q}}_1 = \begin{bmatrix} 0.2665 & 0.1097 & 0.1363 & 0.9478 \end{bmatrix}^\mathsf{T}$	$\boldsymbol{\omega}_1 = \begin{bmatrix} 0.0011 & -0.0127 & 0.0548 \end{bmatrix}^\mathsf{T}$	rad/s
$\bar{\mathbf{q}}_2 = \begin{bmatrix} 0.2671 & 0.1357 & 0.0978 & 0.9490 \end{bmatrix}^\mathsf{T}$	$\boldsymbol{\omega}_2 = \begin{bmatrix} -0.0062 & 0.0105 & 0.0662 \end{bmatrix}^\mathsf{T}$	rad/s
$\bar{\mathbf{q}}_3 = \begin{bmatrix} 0.2685 & 0.1281 & 0.0890 & 0.9506 \end{bmatrix}^\mathsf{T}$	$\boldsymbol{\omega}_3 = \begin{bmatrix} -0.0086 & 0.0118 & 0.0664 \end{bmatrix}^\mathsf{T}$	rad/s
$\bar{\mathbf{q}}_4 = \begin{bmatrix} 0.2691 & 0.1238 & 0.0857 & 0.9513 \end{bmatrix}^\mathsf{T}$	$\boldsymbol{\omega}_4 = \begin{bmatrix} -0.0094 & 0.0116 & 0.0664 \end{bmatrix}^\mathsf{T}$	rad/s
$\bar{\mathbf{q}}_5 = \begin{bmatrix} 0.2693 & 0.1214 & 0.0842 & 0.9517 \end{bmatrix}^\mathsf{T}$	$\boldsymbol{\omega}_5 = \begin{bmatrix} -0.0098 & 0.0114 & 0.0665 \end{bmatrix}^\mathsf{T}$	rad/s
$\bar{\mathbf{q}}_6 = \begin{bmatrix} 0.2694 & 0.1199 & 0.0833 & 0.9519 \end{bmatrix}^\mathsf{T}$	$\boldsymbol{\omega}_6 = \begin{bmatrix} -0.0100 & 0.0112 & 0.0665 \end{bmatrix}^\mathsf{T}$	rad/s
$\bar{\mathbf{q}}_7 = \begin{bmatrix} 0.2696 & 0.1179 & 0.0822 & 0.9522 \end{bmatrix}^\mathsf{T}$	$\boldsymbol{\omega}_7 = \begin{bmatrix} -0.0103 & 0.0109 & 0.0665 \end{bmatrix}^\mathsf{T}$	rad/s
$\bar{\mathbf{q}}_8 = \begin{bmatrix} 0.2696 & 0.1184 & 0.0825 & 0.9521 \end{bmatrix}^\mathsf{T}$	$\boldsymbol{\omega}_8 = \begin{bmatrix} -0.0103 & 0.0109 & 0.0665 \end{bmatrix}^\mathsf{T}$	rad/s
$\bar{\mathbf{q}}_9 = \begin{bmatrix} 0.2695 & 0.1190 & 0.0828 & 0.9520 \end{bmatrix}^\mathsf{T}$	$\boldsymbol{\omega}_9 = \begin{bmatrix} -0.0102 & 0.0110 & 0.0665 \end{bmatrix}^\mathsf{T}$	rad/s

A constant disturbance torque of 0.01 N · m is included in some of the simulations to analyze the relative performance of the controllers in the presence of un-modelled effects. The magnitude of the torque was chosen to create steady-state angular errors that are well above the integration tolerance to allow for easier performance comparisons. The axis defining the direction of the torque was generated randomly, so that each spacecraft would have a different tracking error. Table 6.2 displays the constant disturbance torques applied to the spacecraft during the simulation.

Table 6.2: Constant disturbance torques applied to the spacecraft throughout the simulation

$$\mathbf{g}_{d_1} = \begin{bmatrix} -0.0025 & -0.0097 & 0.0007 \end{bmatrix}^{\mathsf{T}} \text{ N} \cdot \text{m} \quad \mathbf{g}_{d_2} = \begin{bmatrix} 0.0017 & -0.0068 & 0.0071 \end{bmatrix}^{\mathsf{T}} \text{ N} \cdot \text{m}$$
$$\mathbf{g}_{d_3} = \begin{bmatrix} 0.0096 & -0.0003 & 0.0027 \end{bmatrix}^{\mathsf{T}} \text{ N} \cdot \text{m} \quad \mathbf{g}_{d_4} = \begin{bmatrix} 0.0023 & -0.0024 & 0.0094 \end{bmatrix}^{\mathsf{T}} \text{ N} \cdot \text{m}$$
$$\mathbf{g}_{d_5} = \begin{bmatrix} -0.0026 & 0.0096 & -0.0006 \end{bmatrix}^{\mathsf{T}} \text{ N} \cdot \text{m} \quad \mathbf{g}_{d_6} = \begin{bmatrix} -0.0025 & 0.0007 & 0.0007 \end{bmatrix}^{\mathsf{T}} \text{ N} \cdot \text{m}$$
$$\mathbf{g}_{d_7} = \begin{bmatrix} -0.0025 & -0.0097 & 0.0007 \end{bmatrix}^{\mathsf{T}} \text{ N} \cdot \text{m} \quad \mathbf{g}_{d_8} = \begin{bmatrix} 0.0017 & -0.0068 & 0.0071 \end{bmatrix}^{\mathsf{T}} \text{ N} \cdot \text{m}$$
$$\mathbf{g}_{d_9} = \begin{bmatrix} 0.0096 & -0.0003 & 0.0027 \end{bmatrix}^{\mathsf{T}} \text{ N} \cdot \text{m}$$

The coordination architecture analysis is simplified by maintaining a constant ratio for the proportional and derivative formation-keeping behavior weights. The derivative behavior weight used is determined by

$$\rho^d = \frac{k_d}{k_p}\rho^p = \frac{3}{5}\rho^p \tag{6.8}$$

This restriction provides for similar convergence characteristics in the relative and absolute angular errors of the spacecraft formation.

Two measures of the angular error of the formation are calculated for each simulation. The absolute angular error is the average angular difference between the spacecraft in the formation and the absolute desired attitude. The relative angular error is the average angular difference between the spacecraft in the formation.

6.2 Nominal Case

The first simulation presented in this chapter is used to validate the stability and convergence analysis presented in the previous chapter. A five-spacecraft formation is simulated with no un-modelled effects (i.e. no disturbance torques). The formation uses a coordination architecture with two connections per spacecraft, $c = 2$. A moderate proportional behavior weighting of

$$\rho^p = 1.5 \tag{6.9}$$

is used in the simulation.

Figure 6.2 contains three plots showing the results of the simulation. The average relative angular error between the spacecraft is shown in the top plot. The middle plot shows the average absolute angular error of the spacecraft in the formation. The magnitude of the control torque averaged over the spacecraft in the formation is plotted in the bottom plot.

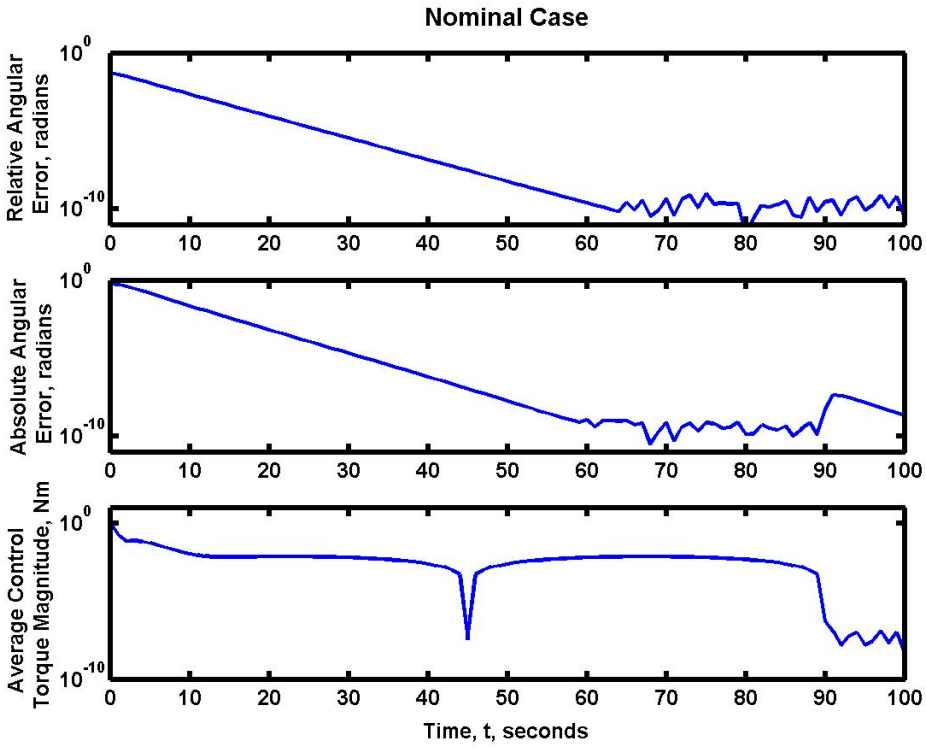

Figure 6.2: The simulation results of a spacecraft formation using the quaternion-based decentralized controller

The simulation results validate the stability and convergence analysis in the previous chapter. The plots in Figure 6.2 show that the spacecraft formation converges to the reference attitude trajectory, as is expected in the absence of disturbing effects. The relative and absolute angular errors fall below the integration tolerance in approximately 65 seconds. The control torque magnitude follows a generally well-behaved "bang-bang" type path until the maneuver is completed. At approximately 90 seconds, the control torque magnitude falls to the integration tolerance, which represents the completion of the slew maneuver.

6.3 Differing Coordination Architectures

The performance of different coordination architectures is investigated in this section. As described in the previous chapter, coordination architectures can vary by the strength of the connections and the number of connections between spacecraft. The effects of varying both of the coordination architecture parameters are investigated using simulations including a constant un-modelled disturbance torque. The spacecraft formation will have a steady state angular error due to the un-modelled torque because the control law does not include an integral control term. The performance of the different coordination architectures is based on the magnitude of the steady state angular errors of the formation.

6.3.1 Behavior Weighting Variation

The effect of varying the strength of the connections between the spacecraft in the formation is investigated in this section. Seven simulations of a five-spacecraft formation are performed. The initial attitude states and the constant disturbance torques defined for Sat 1 through 5 in Section 6.1 are used for the simulations. Each simulation uses a two-connection coordination architecture. All of the connections are equally weighted. The simulations differ by the magnitude of the formation-keeping behavior weight used. Proportional behavior weights ranging from 0 to 2.5 in 0.5 increments are used in the first six simulations. The seventh simulation uses a 2.9 behavior weight (a 3.0 behavior weight would violate Eq. (5.4)).

The results of the simulations are presented in Figures 6.3, 6.4, and 6.5. A log scale is used on the ordinate axis of the plots in the figures to better show the characteristics of the curves. The relative angular error of the spacecraft formation is shown in Figure 6.3, and

the absolute angular error is shown in Figure 6.4.

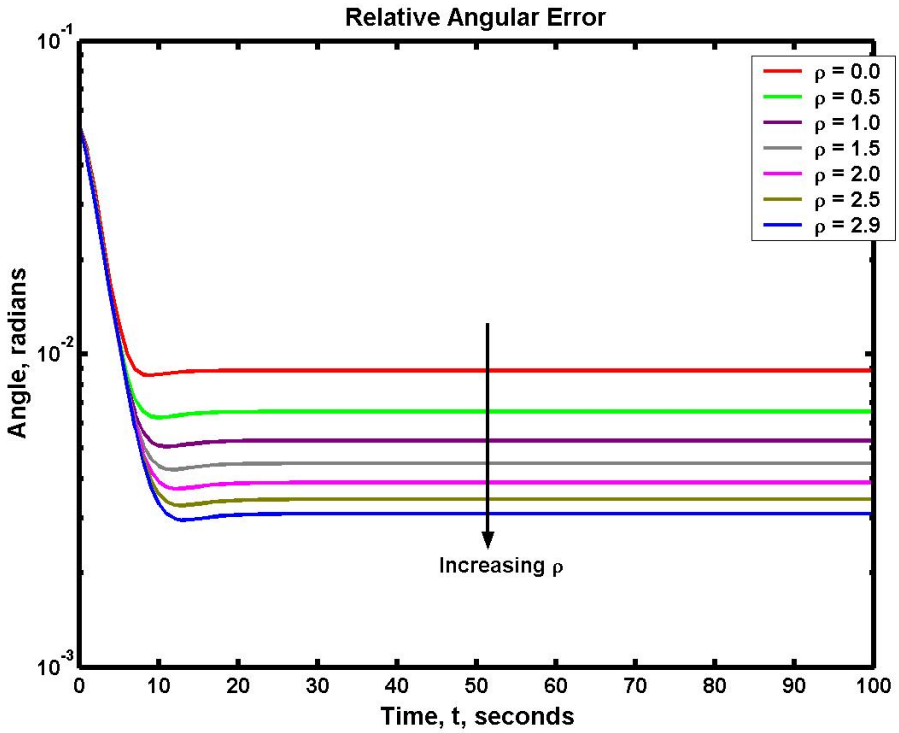

Figure 6.3: Relative angular error performance of the spacecraft formation using different values of the formation-keeping behavior weighting

The angular error plots, Figures 6.3 and 6.4, show that the steady state relative and absolute angular errors of the formation decrease with an increasing connection strength. The improvement of the steady-state relative angular error is expected with the increased weighting of the formation-keeping behavior. However, the improvement in the absolute angular error is an unexpected benefit of the stronger connections. The steady state angular errors found in the simulations are summarized in Table 6.3.

Figure 6.5 contains a semi-log plot of the control torque magnitude averaged over the spacecraft in the formation during the simulation. Only one curve is visible because the results for the seven simulations are nearly identical.

The simulation results lead to the conclusion that the overall performance of the coordinated attitude controller is improved with stronger connections between the spacecraft. Furthermore, the performance boost does not require an increase in the average control effort used

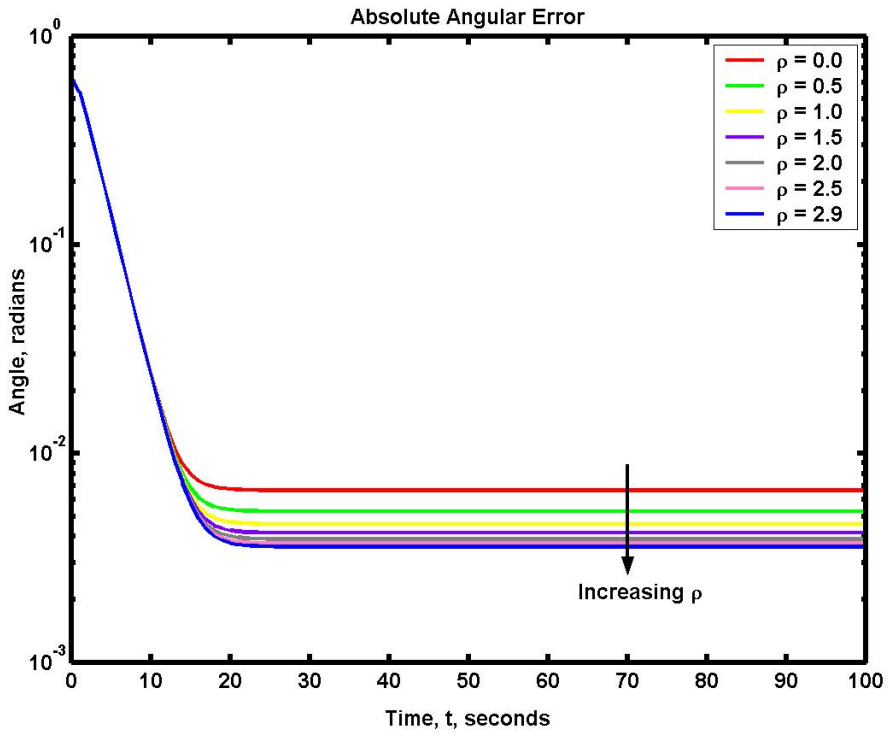

Figure 6.4: Absolute angular error performance of the spacecraft formation using different values of the formation-keeping behavior weighting

Table 6.3: Steady state angular errors for the different formation-keeping behavior weights

Behavior Weighting (ρ^p)	Absolute Angular Error (deg)	Relative Angular Error (deg)
0.00	6.7×10^{-3}	8.9×10^{-3}
0.50	5.3×10^{-3}	6.5×10^{-3}
1.00	4.6×10^{-3}	5.3×10^{-3}
1.50	4.2×10^{-3}	4.5×10^{-3}
2.00	3.9×10^{-3}	3.9×10^{-3}
2.50	3.7×10^{-3}	3.5×10^{-3}
2.99	3.6×10^{-3}	3.1×10^{-3}

by the spacecraft.

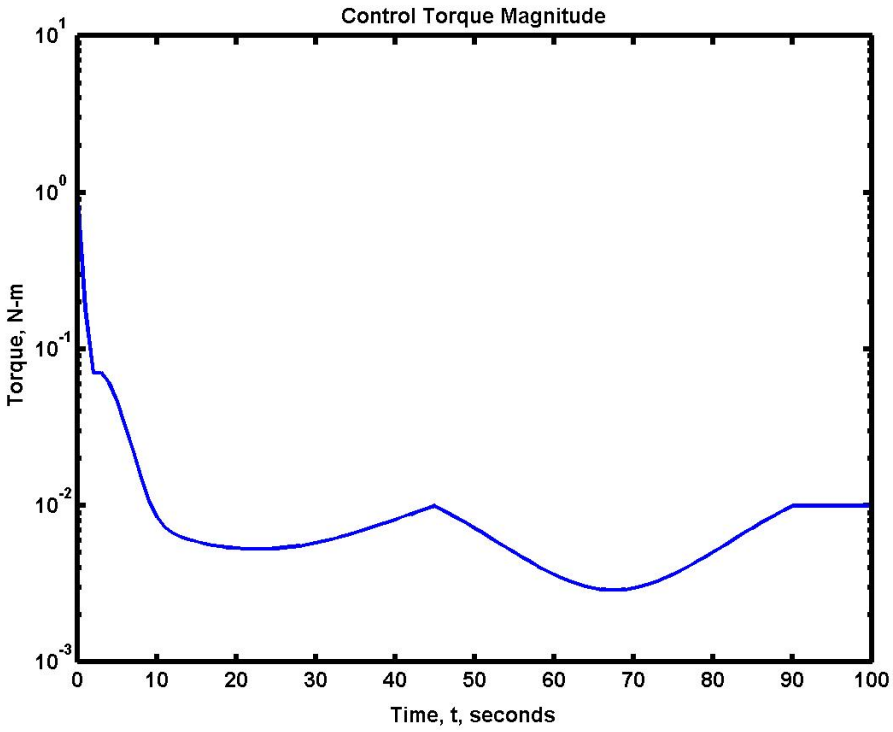

Figure 6.5: Average control torque magnitude applied by the spacecraft in the formation using different values of the formation-keeping behavior weighting

6.3.2 Spacecraft Connection Variations

Coordination architectures can differ in the number of connections used. The effects of varying the number of connections in a coordination architecture are investigated using simulations of a six-spacecraft formation. As in the simulation in the previous section, the spacecraft in the formation are subjected to a constant disturbance torque. The initial attitude states and the constant disturbance torques defined for Spacecraft 1 through 6 in Section 6.1 are used for the simulations. The connection strengths are the same for all of the simulations. A moderate connection strength of

$$\rho^p = 1.5 \tag{6.10}$$

is used in the simulations. Five simulations are performed with 0, 2, 3, 4 and 5 connections per spacecraft. The one-connection case is omitted because that coordination architecture does not link the formation entirely. Diagrams A through D of Figure 5.1 depict the 0, 2, 3, and 4-connection coordination architectures.

Figures 6.6 and 6.7 show the angular error results for the five simulations. The relative angular error during the simulation is plotted in Figure 6.6, and the absolute angular error is plotted in Figure 6.7. The plots show that the steady-state absolute and relative angular errors decrease with a larger number of connections per spacecraft. The increase in relative attitude performance is expected with a greater number of connections. The increase in attitude information leads to a better estimate of the "average" attitude of the formation. The absolute attitude performance is increased with a greater number of connections between the spacecraft. The steady state angular errors for each simulation are displayed in Table 6.4.

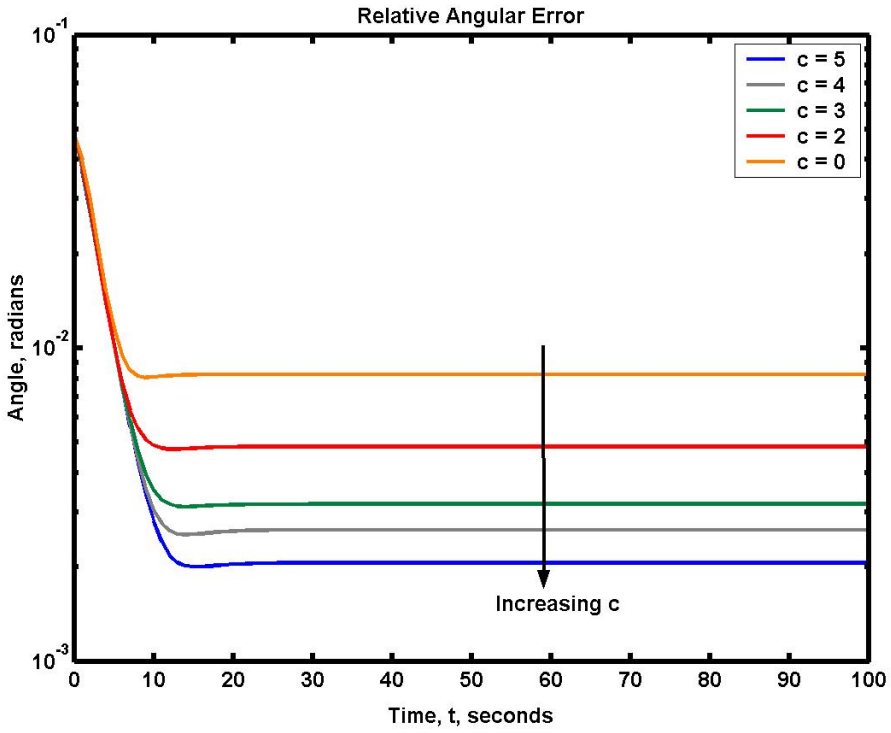

Figure 6.6: Relative angular error performance of the spacecraft formation using different numbers of connections between spacecraft

The table clearly shows the decrease in the steady state angular errors with an increasing number of connections per spacecraft. The angular errors seem to decrease asymptotically as the completely connected coordination architecture case is reached.

The control torque magnitude averaged over the formation for the simulations is plotted in Figure 6.8. Only one curve is visible in the plot because the differences in the average control effort are indiscernible between the simulations. These simulation results lead to

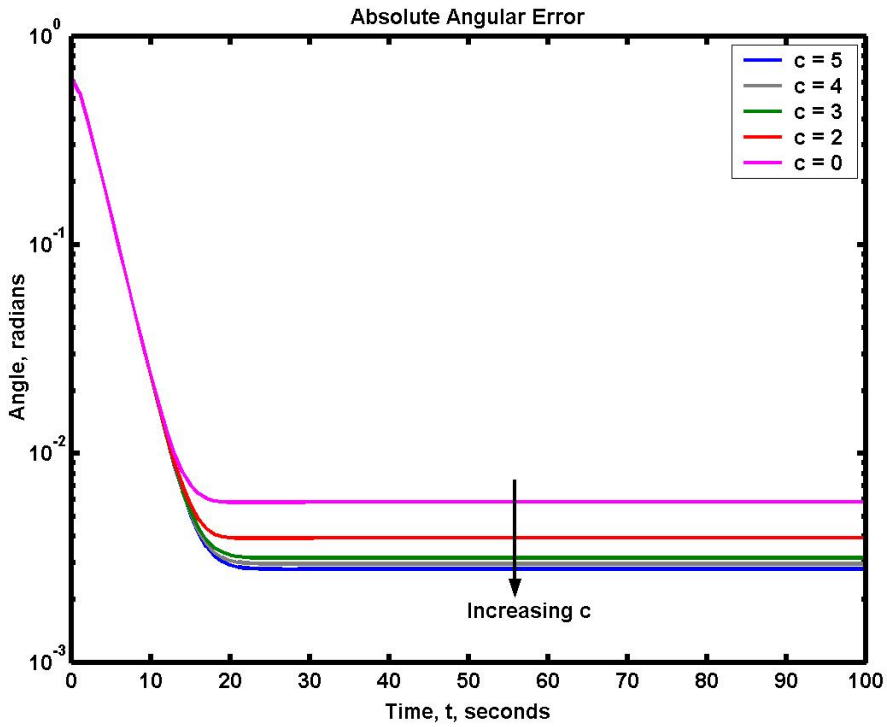

Figure 6.7: Absolute angular error performance of the spacecraft formation using different numbers of connections between spacecraft

Table 6.4: Steady state angular errors for the different coordination architectures

Number of Connections (c)	Absolute Angular Error (deg)	Relative Angular Error (deg)
0	5.9×10^{-3}	8.4×10^{-3}
2	3.9×10^{-3}	4.9×10^{-3}
3	3.2×10^{-3}	3.2×10^{-3}
4	2.9×10^{-3}	2.7×10^{-3}
5	2.8×10^{-3}	2.1×10^{-3}

the conclusion that a greater number of connections per spacecraft increases the overall performance of the spacecraft formation, while not requiring any greater average control effort.

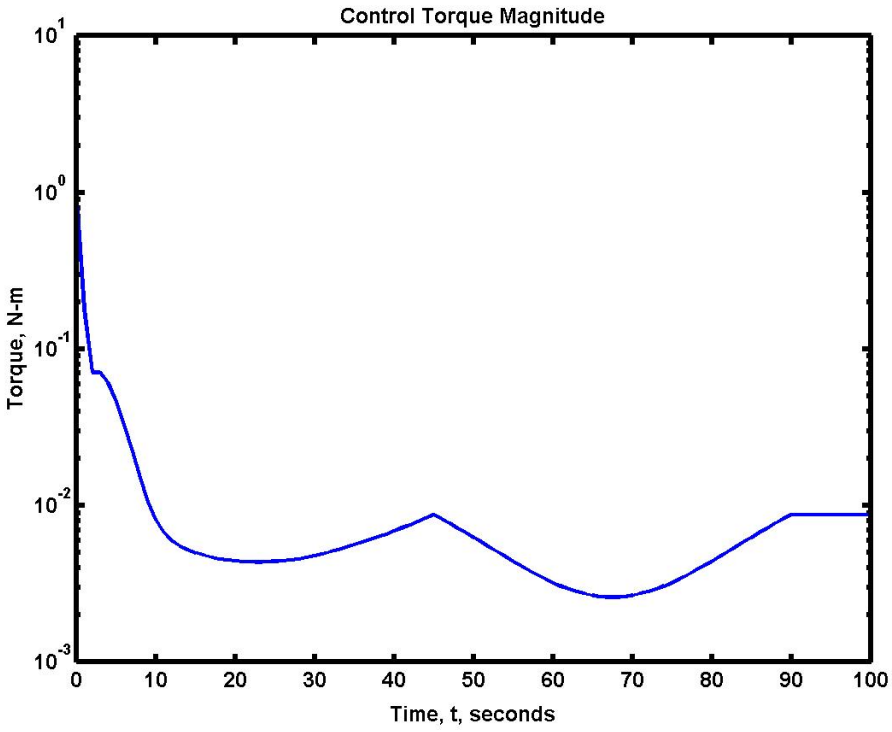

Figure 6.8: Average control torque magnitude applied by the spacecraft in the formation using different numbers of connections between spacecraft

6.3.3 Cluster Coordination Architectures

The performance of the cluster coordination architecture introduced in the previous chapter is investigated by simulating a nine-spacecraft formation. The spacecraft are divided into three clusters of three spacecraft. Within a cluster, the spacecraft are strongly connected. The clusters are connected through weak connections between spacecraft in different clusters. The cluster architecture used is depicted in Figure 5.4. Table 6.5 shows the connections used in the cluster architecture simulated. A strong connection is denoted by an "S," while a weak connection is denoted by a "W." The absence of a connection is denoted by a "0." Only the upper-right corner of the table is completed because Eq. (5.6) requires that the table is symmetric about its diagonal. The proportional behavior weight for the strong connections is

$$\rho^p = 2.990 \tag{6.11}$$

and the behavior weight for the weak connections is

$$\rho^p = 0.500 \tag{6.12}$$

Table 6.5: The coordination architecture table for a cluster architecture

Sat No.	1	2	3	4	5	6	7	8	9
1	0	S	S	W	0	0	0	0	0
2	-	0	S	0	0	0	0	W	0
3	-	-	0	0	W	0	W	0	0
4	-	-	-	0	S	S	0	0	0
5	-	-	-	-	0	S	W	0	0
6	-	-	-	-	-	0	0	0	W
7	-	-	-	-	-	-	0	S	S
8	-	-	-	-	-	-	-	0	S
9	-	-	-	-	-	-	-	-	0

The results of the simulation are presented in Figure 6.9. The relative angular error is shown in the top plot. The center plot shows the absolute angular error throughout the simulation. The average control torque magnitude is shown in the bottom plot. Approximately 60 seconds into the simulation the absolute and relative angular errors fall below the integration tolerance, signifying convergence of the formation to reference attitude trajectory. The average control torque magnitude drops below the integration limit at 90 seconds, which is the end of the slew maneuver.

The cluster simulation is performed again with the addition of constant disturbance torques (Table 6.2) to further analyze the performance of the individual clusters and the formation. Figures 6.10 and 6.11 show the relative and absolute angular errors of the clusters and the formation throughout the simulation. Only three curves are visible because Clusters 2 and 3 have nearly identical angular error results. The relative angular error plot shows that the relative alignment of the spacecraft within clusters is better than the relative alignment of the formation as a whole. The strong connections between spacecraft in the same cluster account for this result. The absolute error results for Cluster 3 show that the steady-state

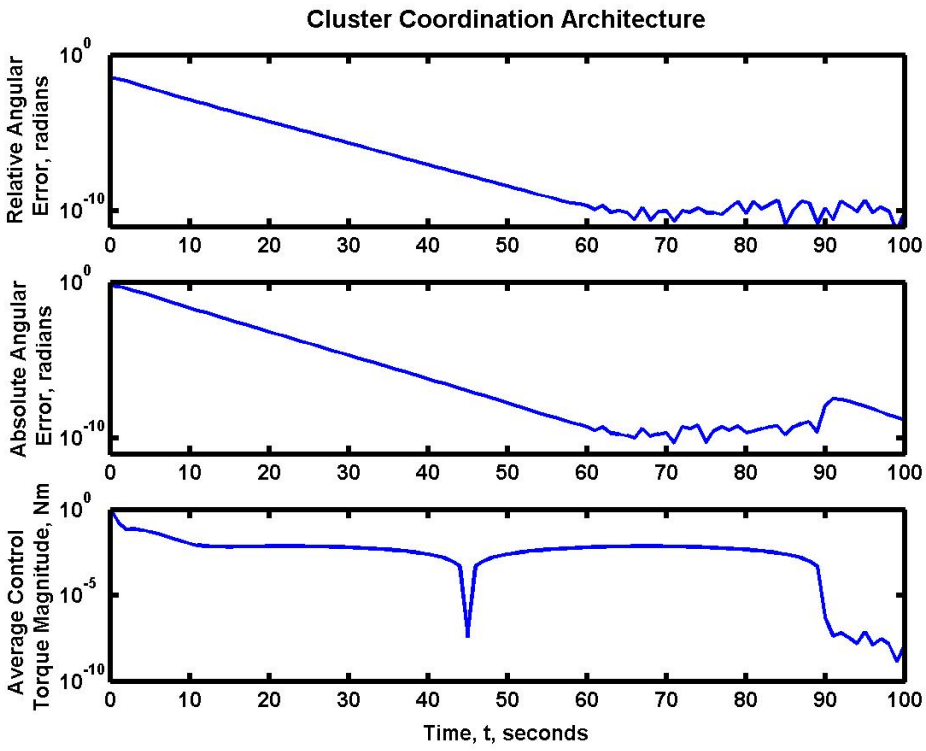

Figure 6.9: Simulation results of a spacecraft formation using a cluster-type coordination architecture

absolute angular error can be adversely affected by the increased importance of relative alignment within the cluster. The average control torque magnitude for the clusters and the overall formation throughout the simulation is presented in Figure 6.12. The control torque magnitude is shown to be settling to the disturbance torque magnitude, 0.01 $\mathrm{N} \cdot \mathrm{m}$, near the end of the simulation.

Although a practical application may not be immediately apparent, the simulations of the cluster architecture show that the class of decentralized coordinated attitude control laws is extremely flexible. The ability to use different coordination architectures allows the formation to be optimized for the specific requirements of a given mission.

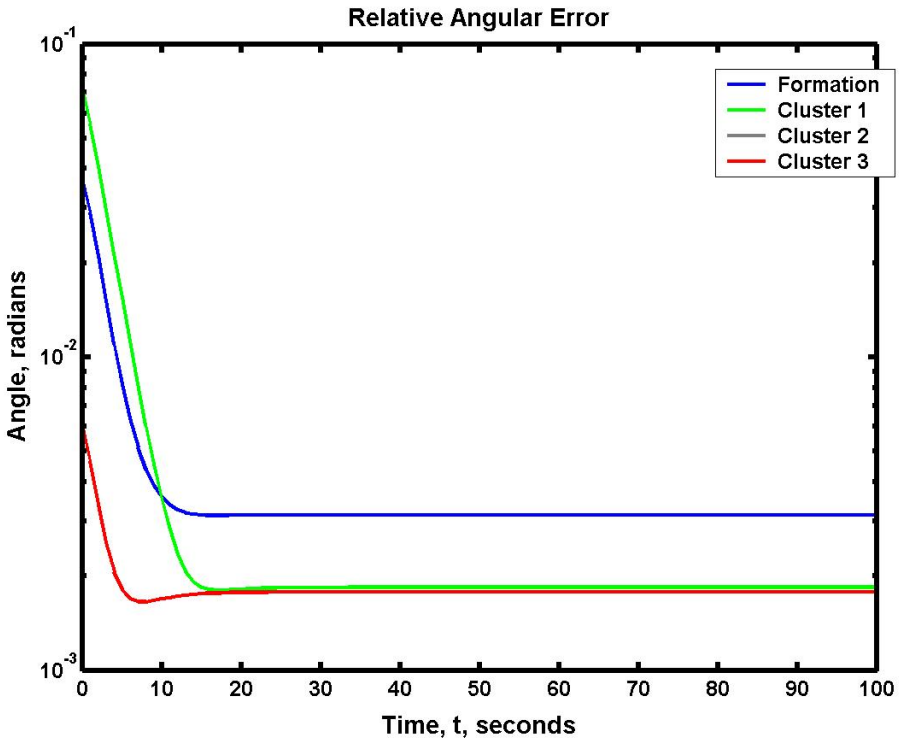

Figure 6.10: Relative angular error results of a spacecraft formation using a cluster-type coordination architecture

6.4 Gravity-Gradient Torque

Most of the simulations presented in this chapter included an un-modelled constant disturbance torque. Although useful in analyzing some performance characteristics, constant disturbance torques are not usually encountered in "real world" applications. Therefore, an un-modelled time-varying disturbance torque is included in the simulations presented in this section. Two simulations are performed. The spacecraft formation in the first simulation is completely unconnected, while a two-connection architecture is used in the second simulation.

A three-spacecraft formation in Low Earth Orbit (LEO) is simulated. The initial orbital elements of the spacecraft are shown in Table 6.6. The position and velocity of the spacecraft are simulated assuming Keplerian orbits.

A prominent disturbance torque experienced by spacecraft in LEO is the gravity-gradient

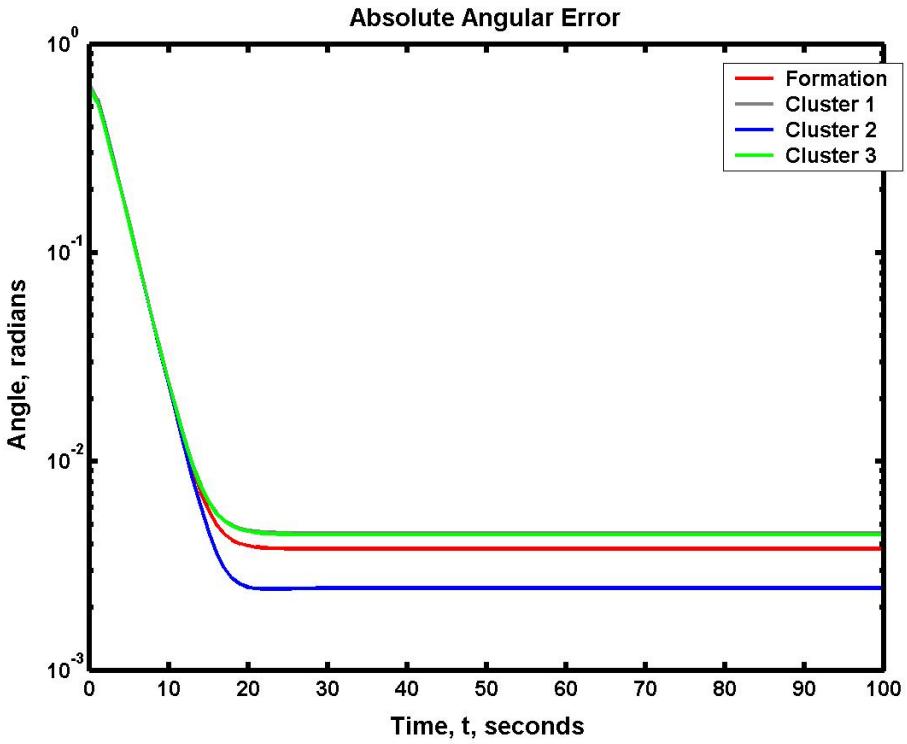

Figure 6.11: Absolute angular error results of a spacecraft formation using a cluster-type coordination architecture

Table 6.6: Initial orbital elements of the spacecraft in the formation

Sat No.	1	2	3
Semi-Major Axis	6778 km	6778 km	6778 km
Eccentricity	1×10^{-5}	1×10^{-5}	1×10^{-5}
Inclination	45^o	45^o	45^o
Right Ascension of the Ascending Node	-0.1^o	0.0^o	0.1^o
Argument of Periapsis	0.0^o	0.0^o	0.0^o
True Anomaly	0.0^o	0.0^o	0.0^o

torque. The gravity-gradient torque is calculated using

$$\mathbf{g}_d = 3\frac{\mu}{r^3}\mathbf{o}_3^{\times}\mathbf{I}\mathbf{o}_3 \tag{6.13}$$

where μ is Earth's gravitational constant, r is the distance from the center of the Earth,

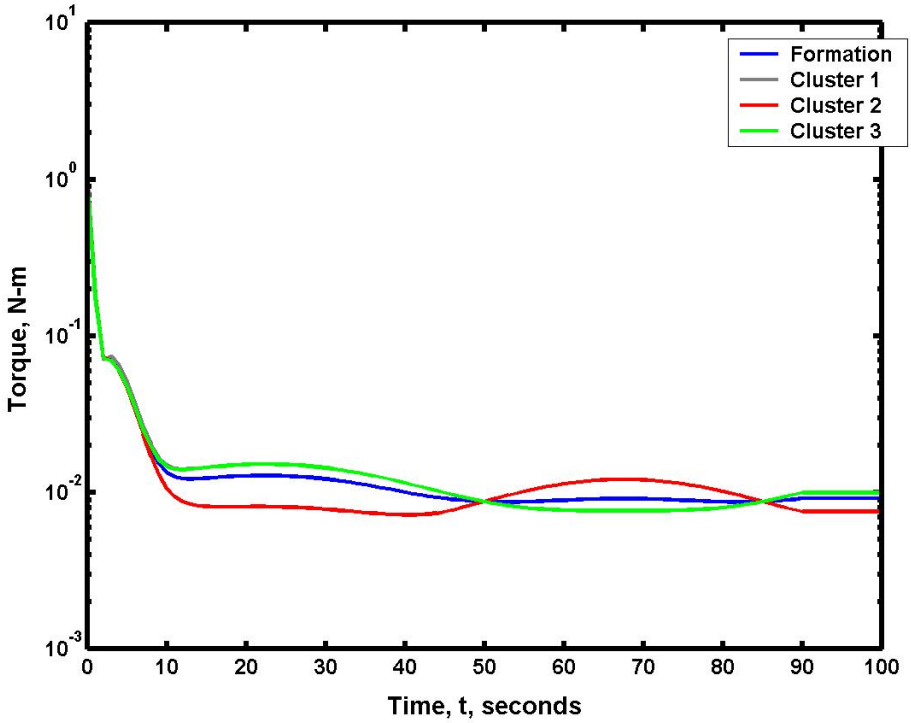

Figure 6.12: Control torque magnitude averaged over the spacecraft formation during a simulation using a cluster-type coordination architecture

and $\mathbf{o}_3$ is the third column of the rotation matrix $\mathbf{R}^{bo}$, which represents the rotation from the orbital to the body-fixed reference frame. The origin of the orbital reference frame is located at the center of mass of the spacecraft. The orientation of the orbital reference frame is defined so that the 3-axis is directed toward the center of the Earth, the 2-axis is in the orbit normal direction, and the 1-axis is normal to the 2 and 3-axes.

The motion of the reference spacecraft is altered to better analyze the performance of the controller. The simulations use a reference spacecraft that performs a 270^o slew in 1000 seconds. The reference spacecraft then maintains its attitude for 1700 seconds after performing the slew maneuver. The total simulation duration is 45 minutes, which is approximately half an orbital period.

The disturbing effects of the gravity-gradient torque are increased in the simulation by

increasing the moments of inertia of the spacecraft in the formation to

$$\mathbf{I} = \begin{bmatrix} 200 & 0 & 0 \\ 0 & 300 & 0 \\ 0 & 0 & 400 \end{bmatrix} \; kg \cdot m^2 \tag{6.14}$$

In the second simulation a two-connection coordination architecture is used by the spacecraft formation. The proportional formation-keeping weighting is set to

$$\rho^p = 2.5 \tag{6.15}$$

The angular error results of the simulations are presented in Figures 6.13 and 6.14. The average control torque magnitude is shown in Figure 6.15. The blue curves in the plots represent the unconnected case, and the red curves represent the connected case. The results for both simulations show that the gravity-gradient torque introduces oscillations into the spacecraft formation, as is expected with a time-varying torque. As in the case of the constant disturbance torque, the relative alignment of the formation is improved by the incorporation of the formation-keeping behavior. The absolute alignment of the formation is approximately the same for both simulations. The absolute angular error for the connected case drops below the error of the unconnected case briefly at some points of the simulation. The same phenomenon is visible in the average control effort plot.

6.5 Summary

The stability and convergence results presented in the previous chapter were validated using a simulation of a spacecraft formation with no un-modelled effects. The effects of varying two coordination architecture parameters were investigated using simulations including constant un-modelled disturbance torques. The simulation results showed that increasing the strength and number of connections of a coordination architecture provides better attitude performance without increasing the average control effort required. A comparison was performed between a connected and unconnected spacecraft formation in the presence of a time-varying torque. The connected formation had better relative attitude performance and similar absolute attitude performance to the unconnected formation. The results presented in this chapter are used in the next chapter to draw conclusions and to determine areas requiring further research.

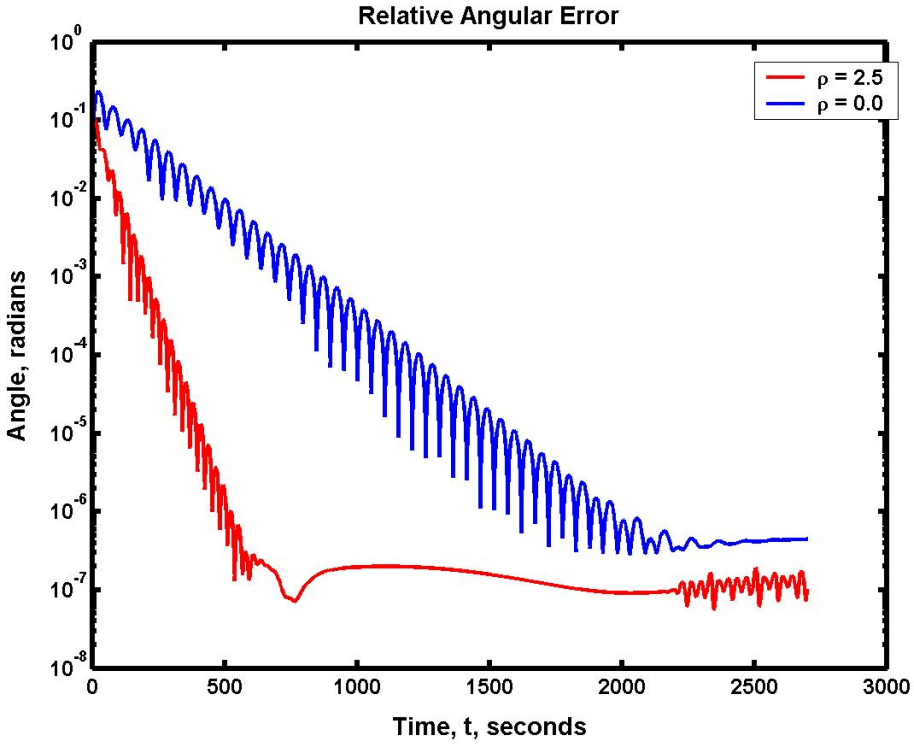

Figure 6.13: Relative angular error results of a spacecraft formation subjected to a gravity-gradient torque

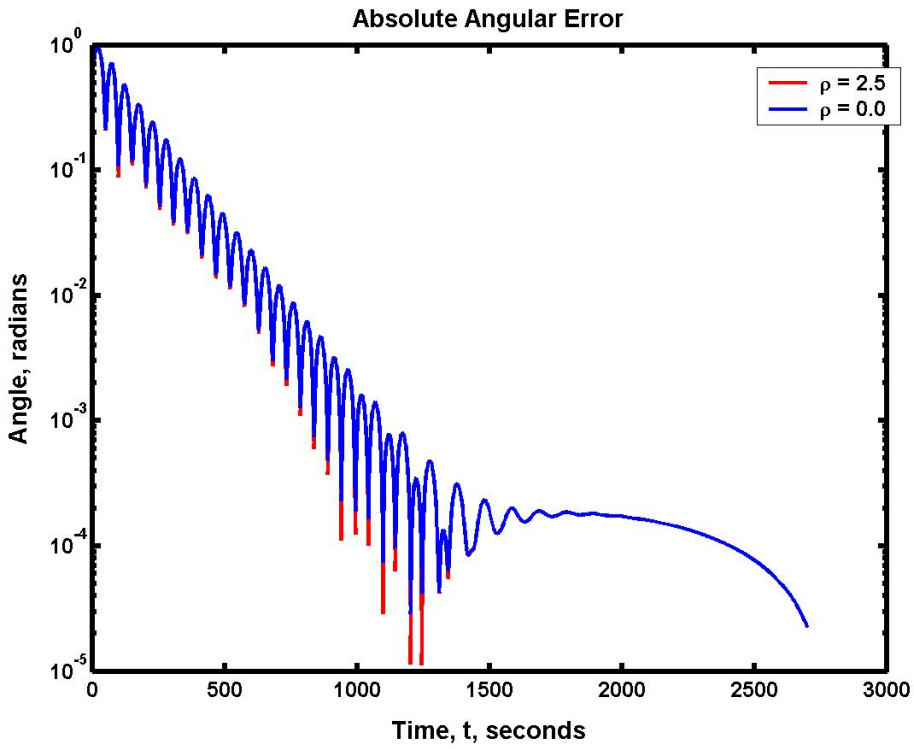

Figure 6.14: Absolute angular error results of a spacecraft formation subjected to a gravity-gradient torque

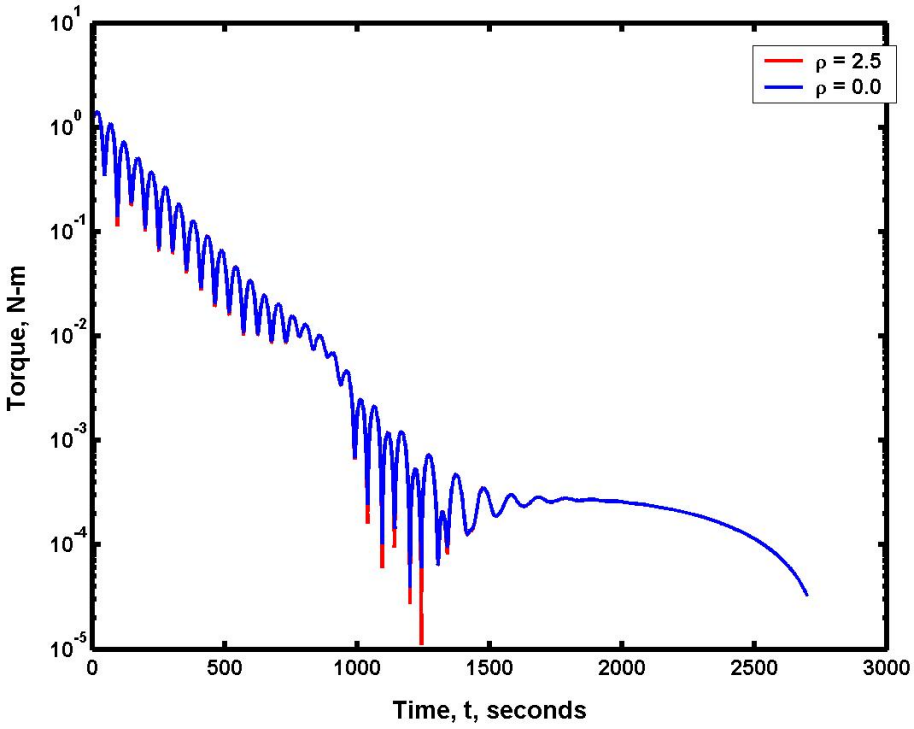

Figure 6.15: Average torque magnitude results of a spacecraft formation subjected to a gravity-gradient torque

Chapter 7

Summary & Conclusions

Spacecraft formations offer more powerful and robust space system architectures than single spacecraft systems. Investigations into the dynamics and control of spacecraft formations are vital for the development and design of future successful space missions. The primary contribution of this work is the development and analysis of a class of decentralized coordinated attitude tracking control laws that guarantee global convergence of a spacecraft formation's attitude.

Special emphasis is placed on developing physically significant relative attitude variables, and providing a global convergence proof for the class of decentralized attitude control laws. These areas are inadequately addressed in prior literature on the topic. The relative attitude quaternion and relative angular velocity vector are developed as physically significant relative attitude variables. These variables are used in the development of the attitude control laws. Lyapunov stability theory is used to prove that the class of decentralized attitude control laws guarantee the global convergence of the spacecraft formation's attitude. The results of a numeric simulation of a five-spacecraft formation performing a slew maneuver reinforced the convergence results.

The class of decentralized attitude control laws consists of control laws that use different coordination architectures. Coordination architectures can vary by the number and strength of the connections between spacecraft. The performance effects of varying these two coordination architecture variables are investigated using numeric simulations of a spacecraft formation with constant applied disturbance torques.

The simulation results show that increasing either the number or strength of the connections decreases the steady-state relative and absolute angular errors caused by the constant disturbance torques without increasing the average control effort required. The decrease in the steady-state relative angular error is expected because with an increase in the number or strength of the connections between spacecraft a greater importance is placed on the relative alignment by the decentralized attitude control laws. However, the decrease in the steady-state absolute angular error is unexpected. The gravity-gradient torque simulation results further complicate this matter. In that simulation, an increase in the number and strength of the connections leads to better relative alignment, but does not provide any absolute alignment benefit.

The physical reasoning behind the results for the absolute alignment in the different simulations is not readily apparent, and warrants further investigation. Analytic analysis into the effects of un-modelled disturbance torques on the formation may be useful in determining the cause of this phenomenon. Another area for further analysis is the effect of imperfect communication on the performance of the control laws. Particularly interesting would be the use of a sequential filter to alleviate some of the dependency of the control laws on continuous communication between the spacecraft.

During the course of this research the author noted several possible extensions to this work. The first logical extension would be the addition of an integral control term to counteract constant or slow-varying disturbance torques. However, the author is quick to note that the use of an integral control term in the presence of conflicting control aims could lead to situations where the formation-keeping control action is simply cancelled out by a station-keeping integral control term. Possibly the most interesting extension would be the application of the coordinated control approach used in this work to the orbital control of a spacecraft formation. It is believed by the author that the similar form of the relative position variables and the relative attitude variables would also allow several of the analytic techniques used in this work to be applied to the problem.

References

[1] P. Wang and F. Hadaegh, "Coordination and control of multiple microspacecraft moving in formation," *The Journal of the Astronautical Sciences*, vol. 44, pp. 315–355, July-September 1996.

[2] P. Wang, F. Hadaegh, and K. Lau, "Synchronized Formation Rotation and Attitude Control of Multiple Free-Flying Spacecraft," *Journal of Guidance, Control, and Dynamics*, vol. 22, pp. 28–35, January-February 1999.

[3] P. Wang, J. Yeh, and F. Hadaegh, "Synchronized Rotation of Multiple Autonomous Spacecraft with Rule-Based Controls: Experimental Study," *Journal of Guidance, Control, and Dynamics*, vol. 24, pp. 352–359, March-April 2001.

[4] W. Kang, A. Sparks, and S. Banda, "Coordinated Control of Multisatellite Systems," *Journal of Guidance, Control, and Dynamics*, vol. 24, pp. 360–368, March-April 2001.

[5] W. Kang and H.-H. Yeh, "Co-ordinated attitude control of multi-satellite systems," *International Journal of Robust and Nonlinear Control*, vol. 12, pp. 185–205, February-March 2002.

[6] W. Kang, N. Xi, and A. Sparks, "Theory and applications of formation control in a perceptive referenced frame," in *Proceedings of the IEEE Conference on Decision and Control*, (Sidney), December 2000.

[7] W. Kang, H.-H. Yeh, and A. Sparks, "Coordinated Control of Relative Attitude for Satellite Formation," in *Guidance, Naviagtion, and Control Conference and Exhibit*, (Montreal, Canada), AIAA 2001-4093, August 2001.

[8] W. Kang and A. Sparks, "Coordinated Attitude and Formation Control of Multi-satellite Systems," in *Guidance, Naviagtion, and Control Conference and Exhibit*, (Monterey, California), AIAA 2002-4655, August 2002.

[9] W. Ren and R. W. Beard, "Virtual Structure Based Spacecraft Formation Control with Formation Feedback," in *AIAA Guidance, Navigation, and Control Conference and Exhibit*, (Monterey, California), AIAA 2002-4963, August 2002.

[10] J. Lawton, R. W. Beard, and F. Y. Hadaegh, "Elementary Attitude Formation Maneuvers Via Leader-following and Behavior-based Control," in *Guidance, Naviagtion, and Control Conference and Exhibit*, (Denver, Colorado), AIAA 2000-4442, August 2000.

[11] R. W. Beard, J. Lawton, and F. Y. Hadaegh, "A feedback architecture for formation control," in *American Control Conference*, (Chicago, IL), June 2000.

[12] J. Lawton, B. Young, and R. Beard, "A decentralized approach to elementarty formatoin maneuvers," in *Proceedings of The IEEE International Conference on Robotics and Automation*, (San Fransico, CA), April 2000.

[13] R. Beard, J. Lawton, and F. Hadaegh, "A feedback architecture for formation control," *IEEE Transactions on Control Systems Technology*, vol. 9, no. 6, pp. 777–790, 2001.

[14] J. R. Lawton and R. W. Beard, "Synchronized multiple spacecraft rotations," *Automatica*, vol. 38, pp. 1359–1364, August 2002.

[15] A. Das, R. Cobb, and M. Stallard, "TechSat 21 - A Revolutionary Concept in Distributed Space Based Sensing," in *Proceedings of the guidance, navigatin and control conference*, vol. AIAA-98-5255, (Boston, MA), pp. 1–6, AIAA, August 1998.

[16] J. Leitner, F. Bauer, D. Folta, M. Moreau, R. Carpenter, and J. How, "Formation Flight in Space," *GPS World*, February 2002.

[17] A. DeCou, "Orbital station-keeping for multiple spacecraft interferometry," *Journal of the Astronautical Sciences*, vol. 39, pp. 283–297, July-September 1991.

[18] E. Davison, "The Decentralized Stabilization and Control of a Class of Unknown Non-Linear Time-Varying Systems," *Automatica*, vol. 10, pp. 309–316, 1974.

[19] M. Aoki and M. T. Li, "Partial Reconstruction of State Vector in Decentralized Dynamic Systems," *IEEE Transactions on Automatic Control*, vol. 18, pp. 289–292, June 1973.

[20] T. Balch and R. C. Arkin, "Behavior-Based Formation Control for Multirobot Teams," *IEEE Transactions on Robotics and Automation*, vol. 14, pp. 926–939, December 1998.

[21] C. Lindensmith (Ed.), "Technology Plan for the Terrestrial Planet Finder," JPL Publication 03-007, NASA Jet Propulsion Laboratory, California Institute of Technology, Pasadena, California, March 2003.

[22] K. Alfriend, "Dynamics and Control of Formation Flying Satellites." Virginia Tech Aerospace and Ocean Engineering Department Graduate Seminar, September 18 2003.

[23] P. C. Hughes, *Spacecraft Attitude Dynamics*. New York: John Wiley and Sons, 1986.

[24] C. D. Hall, "Class Notes - Spacecraft Attitude Dynamics and Control." January 12, 2003.

[25] H. Schaub and J. L. Junkins, *Analytical Mechanics of Space Systems*. AIAA Education Series, Reston, Virginia: American Institute of Aeronautics and Astronautics, 2003.

[26] H. K. Khalil, *Nonlinear Systems*. New York, New York: MacMillan, 1992.

[27] R. Mortensen, "A Globally Stable Linear Attitude Regulator," *International Journal of Control*, vol. 8, pp. 297–302, 1968.

[28] P. Tsiotras, "New Control Laws for the Attitude Stabilization of Rigid Bodies," in *13th IFAC Symposium on Automatic Control in Aerospace*, pp. 316–321, September 1994.

[29] R. L. Burden and J. D. Faires, *Numerical Analysis 7th Edition*. Pacific Grove, California: Brooks/Cole, 2001.

Vita

Matthew Clark VanDyke was born in Havre de Grace, Maryland. He attended Rising Sun High School, where he graduated in June 1998 with honors. Matt started at Virginia Tech in the Fall of 1998. He received his bachelor's degree in Aerospace Engineering in Spring 1999.